AD-A068 909 PRATT AND WHITNEY AIRCRAFT GROUP WEST PALM BEACH FL G--ETC F/G 11/6
PLASTIC FLOW AND FRACTURE PROCESSES IN POWDER METALLURGICAL NIC--ETC(U)
APR 79 C C LAW, M J BLACKBURN F49620-77-C-0083
UNCLASSIFIED PWA-FR-11749 AFOSR-TR-79-0612 NL

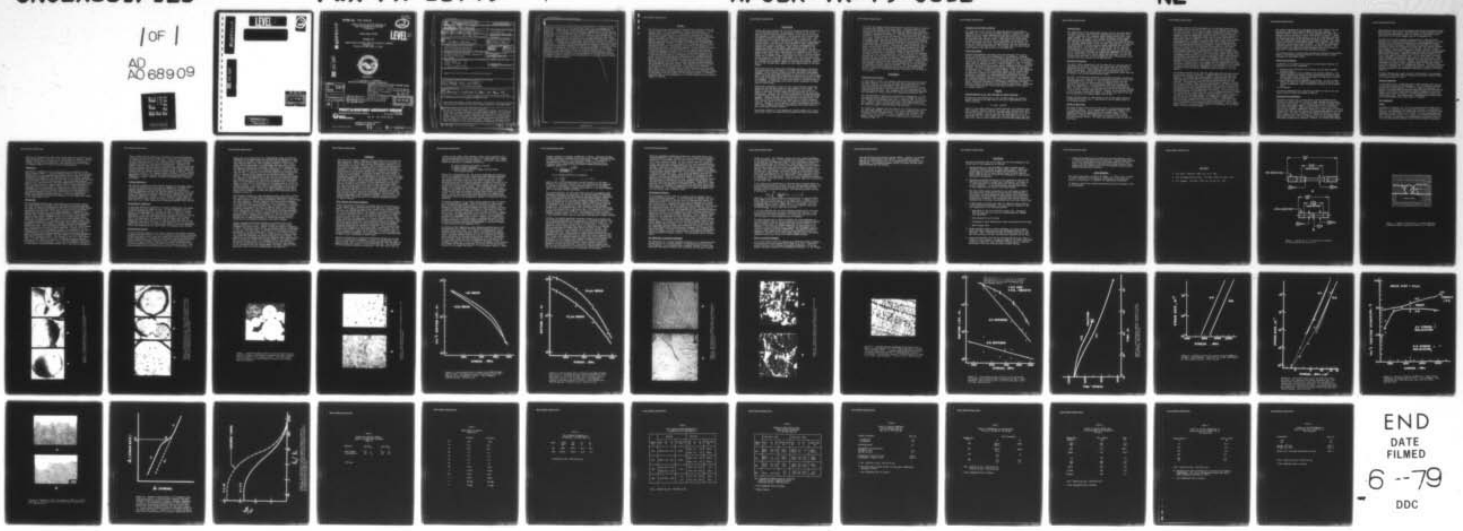

END
DATE FILMED
6 -79
DDC

LEVEL II

2

FR 11769
April 1979

AFOSR-TR- 79-0612

PLASTIC FLOW AND FRACTURE PROCESSES IN POWDER METALLURGICAL NICKEL-BASE SUPERALLOYS

SECOND ANNUAL REPORT

PREPARED FOR

UNITED STATES AIR FORCE OFFICE OF SCIENTIFIC RESEARCH
BUILDING 140
BOLLING AIR FORCE BASE, DC 20332

PREPARED BY:

C. C. LAW AND M. J. BLACKBURN
MATERIALS ENGINEERING & RESEARCH LABORATORY

PRATT & WHITNEY AIRCRAFT GROUP
Government Products Division
P. O. Box 2691
West Palm Beach, Florida 33402

UNITED TECHNOLOGIES®

REF. NO. EII 79-200-7065-FR

Unclassified

SECURITY CLASSIFICATION OF THIS PAGE (When Data Entered)

REPORT DOCUMENTATION PAGE	READ INSTRUCTIONS BEFORE COMPLETING FORM
1. REPORT NUMBER: AFOSR-TR-79-0612	2. GOVT ACCESSION NO. / 3. RECIPIENT'S CATALOG NUMBER
4. TITLE (and Subtitle): Plastic Flow And Fracture Processes In Powder Metallurgical Nickel-Base Superalloys.	5. TYPE OF REPORT & PERIOD COVERED: Interim Report March 1978 - March 1979
	6. PERFORMING ORG. REPORT NUMBER: FR-11749
7. AUTHOR(s): C. C. Law and M. J. Blackburn	8. CONTRACT OR GRANT NUMBER(s): F49620-77-C-0083
9. PERFORMING ORGANIZATION NAME AND ADDRESS: United Technologies Corporation, Pratt & Whitney Aircraft Group, Government Products Division, W. Palm Beach, FL	10. PROGRAM ELEMENT, PROJECT, TASK AREA & WORK UNIT NUMBERS: 2306/A1, 61102F, A1
11. CONTROLLING OFFICE NAME AND ADDRESS: Air Force Office of Scientific Research/NE, Bolling Air Force Base, D.C. 20332	12. REPORT DATE: April 1979; NUMBER OF PAGES: -51-
14. MONITORING AGENCY NAME & ADDRESS (if different from Controlling Office): 54 pp.	15. SECURITY CLASS. (of this report): Unclassified; 15a. DECLASSIFICATION/DOWNGRADING SCHEDULE

16. DISTRIBUTION STATEMENT (of this Report)

"Approved for Public Release; Distribution unlimited."

17. DISTRIBUTION STATEMENT (of the abstract entered in Block 20, if different from Report)

PWA-FR-11749

18. SUPPLEMENTARY NOTES

Annual rept. no. 2. Mar 78 - Mar 79.

19. KEY WORDS (Continue on reverse side if necessary and identify by block number)

Nickel-Base Superalloys, Powder Metallurgy, Hot Isostatic Pressing, Fracture, Notched Section Properties, Mesh Size, Stress Relaxation, Life Improvement.

20. ABSTRACT (Continue on reverse side if necessary and identify by block number)

The use of fine-mesh powder has been suggested as a method to alleviate the non-metallic inclusion problems in current powder products. In the present study, -325 mesh MERL 76 loose powder was characterized in detail and the properties of the consolidation compared with those of the -80 mesh powder. Higher interstitial contents and some interesting powder microstructures have been observed in the -325 mesh powder. However, no influence of these powder variables on tensile and stress-rupture properties of either fine-

DD FORM 1 JAN 73 1473 EDITION OF 1 NOV 65 IS OBSOLETE

Unclassified 392 887

grain or coarse grain consolidations has been observed. During the course of the first-year and the current second-year efforts in this program, notch-rupture has emerged as an interesting and poorly understood phenomenon. A major effort has, therefore, been directed to the elucidation of the rupture mechanism and to identify important variables. It has been observed that the notch-rupture life of MERL 76, heat treated to a high yield strength but in a 'notch-brittle' condition, is dependent not only on temperature and stress, but is also significantly influenced by the temperature/stress path. Loading at lower temperatures and at high stress rates tend to eliminate the notch sensitivity. Peening also significantly improves the notch-rupture life while other surface treatments:electropolishing and pre-stressing have minor effect. The observed beneficial influence of testing in a vacuum is attributed to the absence of a dynamical interaction of the environment with the deforming material at the notch root, rather than oxidation effect, per se. Based on microstructural observations, creep and stress relaxation behavior, grain boundary sliding is considered a critical element of the fracture mechanism. A fracture criterion based on the accumulation of a critical amount of grain boundary damage is proposed.

ABSTRACT

The use of fine-mesh powder has been suggested as a method to alleviate the non-metallic inclusion problems in current powder products. In the present study, -325 mesh MERL 76 loose powder was characterized in detail and the properties of the consolidation compared with those of the -80 mesh powder. Higher interstitial contents and some interesting powder microstructures have been observed in the -325 mesh powder. However, no influence of these powder variables on tensile and stress-rupture properties of either fine-grain or coarse-grain consolidations has been observed. During the course of the first-year and the current second-year efforts in this program, notch rupture has emerged as an interesting and poorly understood phenomenon. A major effort has, therefore, been directed to the elucidation of the rupture mechanism and to identify important variables. It has been observed that the notch-rupture life of MERL 76, heat treated to a high yield strength but in a 'notch-brittle' condition, is dependent not only on temperature and stress, but is also significantly influenced by the temperature/stress path. Loading at lower temperatures and at high stress rates tend to eliminate the notch sensitivity. Peening also significantly improves the notch-rupture life while other surface treatments:electropolishing and pre-stressing have minor effect. The observed beneficial influence of testing in a vacuum is attributed to the absence of a dynamical interaction of the environment with the deforming material at the notch root, rather than an oxidation effect, per se. Based on microstructural observations, creep and stress relaxation behavior, grain boundary sliding is considered a critical element of the fracture mechanism. A fracture criterion based on the accumulation of a critical amount of grain boundary damage is proposed.

INTRODUCTION

Current and future powerplants for use in Air Force systems require the use of advanced materials. The operational conditions, set by the specific aircraft type and mission profile, in turn control the properties demanded in engine components. The situation can be further complicated by varying requirements with location in a given part. This is especially true in large components such as a turbine disk. The disk rim, which is closest to the gas path, demands superior creep-rupture characteristics. The disk bore, which operates at lower temperatures, requires high tensile strength to resist plastic displacements and maintain an adequate burst margin. High rotational speeds and rim temperatures result in increased engine efficiency and thus the specified material properties noted above must be optimized. Turbine disks operate under cyclic loads; viewed simply, one complete mission corresponds to one fatigue cycle. The ability of a disk to tolerate repeated cycles can be related to engine maintenance and life cycle costs which include inspection, overhaul, replacement, etc. Disk acquisition costs are determined by the process cycle used for disk fabrication. Selection of a minimum cost procedure, capable of achieving the property requirements in the finished disk, impacts the cost effectiveness of the total system.

These three areas of turbine disk technology, performance, durability, and acquisition costs are implicit in current and projected Air Force Programs. Pratt & Whitney Aircraft has also structured a development program which has many common objectives to those of the Air Force Program. One direct method of accomplishing inter-meshing of these programs is through contractural efforts and this document is concerned with one such program. It deals with a basic study aimed at elucidating some of the processes and mechanisms that control certain properties of alloys used in turbine disks.

Nickel-base superalloys, because of their unique elevated temperature properties are used exclusively for high pressure turbine disks. The advent of powder metallurgical (P/M) techniques for such alloys has opened up new areas of alloy composition and processing for study and exploitation. Barriers such as ingot heterogeneity and forging problems in high strength alloys have been circumvented by the powder metallurgy approach. Although several fabrication methods have been proven to be effective, direct consolidation of powders by hot isostatic pressing (HIP) has been shown to be the most cost effective method of disk fabrication. Changes in the raw material (powder) and manufacturing method (HIP) lead to property-structural relationships that differ from the more conventional wrought products.

The overall objective of this program is to gain insight into the processes that control the properties of advanced P/M turbine disk alloys.

The first year program studied stress-rupture characteristics of a series of powder metallurgical nickel-base alloys. Structural features were identified which controlled the creep rates and rupture lives in smooth sections of the selected alloys. The creep and fracture processes could be modeled reasonably satisfactorily. Although some insight into the behavior of notched sections was obtained, it was clear that much remained to be done. Therefore, this study was continued into the second year of the program, albeit modified by another major thrust that had developed in P/M metallurgy. The remarkable homogeneity of P/M materials had led to generally very uniform properties, but small discontinuities can perturb this behavior pattern. Specifically, small non-metallic inclusions have been found to set the minimum fatigue capability of these alloys. Such effects are imperfectly understood at the present time, and in the third year of the present program a definitive study of inclusion effects will be undertaken. A method that has been suggested to reduce the size, and therefore the effect of inclusions, is to reduce the mesh size of the powder selected for component manufacture. Such a reduced mesh size could lead to changes in the properties of consolidated material; increased surface area for example could lead to higher interstitial element levels and poor bonding characteristics. The second year program, therefore, studied the characteristics of fine mesh powder and properties obtained from such material. The results again pointed to notch stress-rupture properties as an area of poor understanding which in turn led to considerable emphasis being placed on the study of this property.

EXPERIMENTAL

Preparation of Materials

The alloy MERL 76 used in the present study was vacuum induction melted and argon atomized. The -80 and -325 mesh powder fractions were separated by screening and small samples taken for characterization. Additional material was outgassed at room temperature prior to filling a pre-evacuated container, the container sealed and consolidated by hot isostatic pressing (HIP). Heat treatments of the consolidated materials were performed in a muffle furnace with temperature control of ±10°C.

The -325 mesh MERL 76 powder was consolidated at temperatures of 1177°C and 1200°C which are below and above the γ' solvus of MERL 76 (1190°C). Two different heat treatments were used, a simple solution and age treatment: 1120°C/2 hr/AC + 760°C/8 hr/AC, and a multi-stage solution and age treatment: 1163°C/2 hr/furnace cooled to 1130°C/OQ + 870°C/40 min/AC + 980°C/45 min/AC + 650°C/24 hr/AC + 760°C/8 hr/AC.

The former heat treatment was also used for the -80 mesh material during the first-year program, the data of which will be compared with those generated from the -325 mesh powder. The latter heat treatment, which is currently used for MERL 76 in other programs, will be used in the present study to evaluate the effect of grain size on creep-rupture behavior of MERL 76.

Specimens and Mechanical Testing

The dimensions of the tensile and creep specimens and notch-rupture specimens (K_t = 3.8) are given in Figure 1a and 1b, respectively. The dimensions of the tensile specimens were similar to those of the creep-rupture specimens. Much of the early creep- and notch-rupture testing was performed under constant loads. Creep strains were continuously recorded from LVDT affixed to the test specimens; the accuracy of the strain measurement was 0.01%. More recently some of the testing, together with tensile and stress relaxation tests, have been performed on a computer controlled MTS machine. The specimen used for stress relaxation studies is the same as that for the creep test.

Analytical Methods

Standard metallographic techniques were used throughout the study to monitor structure and fracture appearance of the material. Scanning microscopy was employed not only to examine powder and fracture surfaces, but also to study nucleation behavior in notched specimens. A sufficiently large stage was available to hold a notched specimen so that the notched region could be examined directly at various stages of a test. A specially developed extraction method was also used to characterize powder particle surfaces. The method, illustrated in Figure 2, consists of dispersing the particles to be studied on a support medium. Carbon is then deposited on these particles. A carbon extraction replica of the surface region is obtained by breaking the carbon film around selected particles and immersing the assembly in a bromine/tartaric acid/methanol solution. The etchant penetrates under the film dissolving the metal but leaving the secondary particles attached to the replica surface. Morphological and structural analysis can be performed in a transmission electron microscope. Additional information on the chemical constitution of powder particle surfaces was obtained by Auger electron spectroscopy. Sputtering of surface layers allowed concentration/depth profiles to be obtained for several elements.

RESULTS

Characterization of the -325 Mesh MERL 76 Powder Particles

The particle size distribution of the -325 mesh powder and -80 mesh powder (produced by the same vendor) can both be approximated by the Weibull equation

$$W = \exp - (d/d_0)^B$$

where W is the weight fraction of powder particles with diameters larger than a specific particle diameter d; d_0 and B are constants which have values of 22.5μm and 1.21 for the -325 mesh powder and 60μm and 1.52 for the -80 mesh powder. From the particle size distribution, it can be calculated that for a given weight, the -325 mesh powder particles have about four times as much surface area as the -80 mesh powder particles.

Microstructure

The compositions of the consolidated -80 mesh and the -325 mesh MERL 76 are given in Table 2 from which two differences should be noted. The -80 mesh composition has a slightly higher hafnium content and a lower oxygen content. As a result of the former difference, primary gamma prime particles are larger in the -80 mesh consolidation than those in the -325 mesh consolidation (Figure 6). As shown in the previous section, the increased oxygen content in the -325 mesh consolidation is related to the larger amount of surface adsorbed oxygen associated with the finer powder particles. The grain sizes of the -80 mesh and the -325 mesh consolidations are 21 μm and 12.4 μm, respectively. It is likely that this difference is attributable to a higher HIP temperature in the case of the coarse powder (although the nominal HIP temperature for both was 1177°C) rather than to the initial powder particle sizes. No such differences have been found in other programs in which consolidation of the two mesh sizes were produced in the same HIP run.

Mechanical Properties

The 704°C tensile properties of the -80 mesh and the -325 mesh MERL 76 consolidations are given in Table 3 which shows that the -80 mesh consolidation has lower yield strength but higher ductility than the fine-powder consolidation. These differences can be correlated with the variations in grain sizes between the two consolidations rather than with an effect of the initial powder particle sizes.

The 704°C stress-rupture properties of the smooth specimens and notched specimens (K_t = 3.8) from the two consolidations are given in Table 4 and plotted graphically in Figure 6. Both the smooth-rupture lives and the ductility of the -80 mesh material are somewhat better than the -325 mesh consolidation. These differences stem from a difference in grain size rather than to a difference in the initial powder particle size. At lower stresses, the notch-rupture lives of the -325 are inferior to those of the -80 mesh consolidation. However, the notch-rupture lives of the -325 mesh consolidation appear to be better than those of the -80 mesh consolidation at stresses higher than 655 MPa.

We may note that there is some scatter in the stress-rupture lives of notched stress rupture bars, a characteristic that we shall return to in following sections.

Effect of Grain Size

The range of grain sizes which one can obtain in HIP-consolidated MERL 76 is rather limited. HIP at temperatures of practical interest below the gamma prime solvus produces grain size of about 12μm. HIP at temperatures above the gamma prime solvus (1190°C) results in rapid grain growth; however, the temperatures are limited by the onset of incipient melting (1200°C). The grain size produced by HIP at 1195°C is about 24μm.

The powder particle surface appearance of the -325 mesh powder and -80 mesh powder are similar, and in both cases, three different morphologies have been observed. The "typical" dendritic morphology (Figure 3a) which is associated with a broad range of powder particle sizes, except the smallest; a granular morphology (Figure 3b) which is usually observed in powder particles of intermediate sizes, and the powder particles with featureless surfaces (Figure 3c). The latter type is only found in small powder particles. As might be expected from these different surface morphologies, three different microstructures of the powder particles have been observed and are shown in Figure 4. Figure 4a shows the dendritic microstructure and the granular microstructure in the bottom particle in Figure 4b. This figure also includes a particle with a mixed granular and dendritic microstructure, from this it appears that both microstructures are closely related. Another type of unusual microstructure is shown in Figure 4c which illustrates a powder particle with a segregation-free surface layer and a core which shows a mixed granular and dendritic microstructure. Both the segregation-free layer and the granular microstructure are thought to be produced with conditions of undercooling at the growing solid-liquid interface during powder solidification. In particular, it is envisaged that the segregation-free layer solidified initially under a high degree of undercooling until the release of heat of fusion raised the temperature of the interface to the near-equilibrium value and normal, segregated dendritic growth in the core ensued.

The surface structure of the -325 mesh powder particles has been studied by extraction replica techniques. A typical result is illustrated in Figure 5 which reveals only a small number of equiaxed particles (500Å diameter) on the powder particle surfaces. These particles have not been identified as yet, for no electron diffraction pattern has been obtained. The morphology, based on previous studies, suggests that they are MC-type carbides. Auger electron spectroscopy of two powder samples, one containing particles with diameters less than 10 μm and the other containing particles with diameters 130-180 μm, reveals little difference in the segregation of alloying elements to the surface. The only discernible difference between the two mesh sizes is in the oxygen and carbon contents, which decreased at a slower rate with surface removal by sputtering in the case of the fine powder sample. The oxygen and nitrogen contents of the -325 mesh and -80 mesh powders, as determined by chromatography, before and after consolidation are given in Table I. This table shows that the oxygen contents of the finer powder particles are higher than the -80 mesh powder both before and after consolidation. This increased oxygen content in the finer powder particles is attributed to the larger amount of surface adsorbed oxygen.

The tensile properties of the fine-grain (12μm grain diameter) and the coarse-grain (24μm grain diameter) MERL 76 were quite similar. An important effect of grain size is on stress rupture life; smooth (K_t=1) specimens results are given in Table 5 and plotted in Figure 8. These results show that the stress-rupture lives of the coarse-grain material are longer than those of the fine-grain material at all stresses. However, the difference becomes small as the stress increases. The stress-rupture ductility of both materials appears to be similar at most test conditions, increasing at higher stresses. At 550 MPa the coarse-grain material exhibits a rather low ductility (less than 2 percent). The notch-rupture lives again show large variations (one to two orders of magnitude) at high stresses for both material conditions.

The recurring scatter in notch-rupture properties resulted in a major effort aimed at elucidating controlling factors in notch location, a topic considered in some detail below.

Notch-Rupture Behavior

In general, the variables which govern the notch-rupture behavior of a material fall into four categories:

(1) Microstructural parameters such as grain size and grain boundary microstructures.
(2) Specimen parameters such as geometry and surface conditions. The former determines the elastic stress concentration factor (K_t) and whether plane-stress (sheet type specimen) or plane-strain (notched bar specimen) condition prevails.
(3) Test parameters such as temperature and stress. As will be shown later, the sequence of applying temperature and load and the rate of load increase also have a significant influence on notch-rupture life.
(4) Environment

The results presented below illustrate the effect of some of the variables in each of these four groups on MERL 76.

Microstructural Parameters

The effect of grain size on notch-rupture life has already been described in a previous section, effect of grain boundary microstructure will only be given here. In the present work, the grain boundary microstructures were changed simply by controlling the rate of cooling in the solution treatment. Rapid cooling by quench in oil (OQ), from a low solution treatment temperature, results in a "notch-brittle" condition whereas relatively slow air cooling (AC) significantly improves the notch-rupture life. The grain boundary microstructures produced by these two heat treatments are shown in Figure 9. Except for the blocky primary gamma prime particles, the grain boundaries in the oil-quenched sample are rather straight and featureless. However, in the air-cooled sample,

gamma prime particles have precipitated along the grain boundaries during the relatively slow cooling. The carbide and boride particles extracted from the grain boundaries are shown in Figure 10. More particles are observed in the air-cooled sample than the oil-quenched one.

The effect of the grain boundary microstructure on crack initiation behavior at the notch surface was studied by testing specimens in vacuum. The tests were interrupted periodically for crack inspection using a scanning electron microscope. Microcracks were detected on the notch surfaces of either the oil-quench or the air-cool heat treated specimens after about 50 hours of testing at 704°C/690 MPa. With the air-cool heat treatment, microcracks nucleated at several locations: at gamma prime/gamma interfaces, within large gamma prime particles, at machining marks and at grain boundaries. Figure 11 illustrates the microcracks at the first three types of nucleation sites. In all three cases, the microcracks propagate transgranularly and normal to the stress axis. Nucleation of microcracks at grain boundaries was seldom observed when test times were less than 120 hours. However, with increased test times, the development of cracks at grain boundaries became increasingly evident and would eventually lead to intergranular fracture. The crack nucleation behavior is different for oil-quenched specimens for microcracks preferentially nucleated at and propagated along grain boundaries, as shown in Figure 12.

The above observations suggest that the "notch-brittle" (oil-quenched) condition is associated with the tendency to form grain boundary cracks at an earlier stage of a test.

Specimen Parameters

In the present study, circumferentially notched specimens with a K_t of 3.8 were used throughout all experiments. The only specimen parameter studied was surface treatment of which four types were examined: as-machined, electropolished, as-machined and prestrained, and as-machined and peened. The effect of these specimen surface treatments on the notch-rupture life is shown in Table 6. Peening dramatically increases the notch-rupture life. Electropolishing or prestraining has little effect on the notch-rupture life or may reduce it slightly.

Test Parameters:

Stress

The effect of stress on the 704°C notch-rupture lives of MERL 76 with either the oil-quenched or air-cooled heat treatment is illustrated in Figure 13. For comparison, the stress-rupture lives of the smooth (K_t=1) specimens are also included in the figure. The oil-quenched material shows notch-rupture lives of 6 to 1 hours as the stress increased from 480 to 860 MPa. In contrast, the corresponding notch-rupture lives of the air-cooled material change by more than two orders of magnitude.

That is, the notch-rupture life of the "notch-sensitive" material is much less stress sensitive than that of the "notch-ductile" material. Another salient feature shown in Figure 13 is that although the oil-quenched material is highly "notch-sensitive", its creep-rupture lives are equal or slightly superior to those of the air-cooled material.

Temperature

The effect of temperature on the notch-rupture life of MERL 76 at 690 MPa is shown in Table 7. The notch-rupture lives of both the oil-quenched material and the air-cooled material decrease by about one order of magnitude when the temperature is increased from 704°C to 788°C. However, decreasing the temperature from 704°C results in very significant increases in notch-rupture lives of both materials. The oil-quenched material ceases to be "notch-sensitive" from room temperatures to below about 650°C. Note the large scatter in rupture lives of the oil-quenched material at 650°C and similar scatter shown in Tables 4 and 5. Such a scatter is considered to be an indication of a transition from "notch-brittle" to "notch-ductile" conditions probably arising from a subtle difference in the loading procedure during a test, rather than due to differences in material or specimen machining procedure. As will be demonstrated below, some heretofore ignored test parameters do have significant effect on the notch-rupture life.

Loading Rate

The conventional procedure for stress-rupture or notch-rupture testing is to equilibrate the specimen at the test temperature before applying the load. The latter is accomplished manually by placing standard weights on a load pan which hangs from one end of a lever while the specimen is connected to the other end. This simple procedure is appropriate for determining the creep- and stress-rupture properties of smooth specimens. However, for a notched specimen, because of the stress concentration at the notch root, plastic deformation can occur locally during loading before the full load is reached. However, the local deformation at the notch root is constrained by an elastic core and subsequent plastic flow is therefore governed by a strain-controlled creep relaxation phenomenon. Typically, the rate of deformation is highest initially and decreases rapidly with time. These considerations indicate that the initial stages of a notch-rupture test will be rather important. Further, since the creep relaxation is a time-dependent process, the magnitude of the local stresses at the notch during loading depends on the relative rates of creep relaxation and the stress increase. In particular, rapid loading would lead to a high stress buildup at the notch which, in turn, results in high plastic deformation rates. The converse is true for a slow loading rate. It is well known that the rate of deformation has an important influence on the relative contribution of various deformation mechanisms. For example, at high temperatures, a slow rate of deformation results in a larger amount of grain-boundary sliding than a high rate of deformation.

Thus, if grain boundary sliding is responsible for the grain-boundary initiated fracture observed in MERL 76, the high rate of loading should be beneficial since it reduces the amount of grain boundary sliding during the initial relaxation. The conventional notch-rupture testing equipment precludes the variations of loading rate. Therefore, the present study was conducted using a servo-hydraulic testing machine with which the loading rate can easily be varied by many orders of magnitude. Notched specimens (K_t=3.8) were equilibrated at 704°C before loading at various rates to a nominal stress of either 550 MPa or 690 MPa. Results are shown in Table 8. At a nominal stress of 550MPa, a very significant improvement of rupture life has been observed at loading rates of 4135 MPa/minute or higher. However, no effect of loading rate is observed at 690 MPa.

Loading Temperature

The relative contribution from different deformation mechanisms depends not only on deformation rate but also on temperature. To study the loading temperature effect, specimens were first equilibrated at a selected temperature and then the load was applied at a slow stress rate of 920 MPa/min until 690 MPa was reached, held at 690 MPa for 0.5 hours before the temperature increase. The stress was maintained during the subsequent temperature increase to 704°C. Results of these tests are given in Table 9, which shows that loading at lower temperatures (up to about 482°C at a "slow" loading rate) eliminates premature notch failure.

Environmental Parameters

As with most mechanical properties at elevated temperatures, environment is expected to play an important role. An inert atmosphere such as a vacuum is usually beneficial. However, as shown in Table 10, the magnitude of the improvement in notch-rupture life is surprising. More importantly, it has also been observed that testing six hours in a vacuum followed by an air test also dramatically increases the notch-rupture life. This observation is consistent with the expectation that the crucial part of a notch test is in the initial stages where most of the deformation takes place. Further, it also suggests that it is the interaction of air (or one of its constituents) during the plastic deformation, rather than oxidation per se, which causes the premature notch failure.

Ancillary Test Results

One of the puzzling aspects of the present study was the relative contrast in smooth and notch behavior. The notch properties showed great differences whereas the smooth section creep tests showed very similar characteristics. As the stress levels in notches are substantially higher than those experienced in smooth sections, additional tests of smooth specimens were conducted at higher stresses. Both creep and stress relaxation behavior of the air-cooled and oil-quenched MERL 76 were measured at 704°C. The stress relaxation data were obtained by straining a creep specimen at a

strain rate of 0.01 per minute to a predetermined strain at which the elongation of the specimen was kept constant and the decrease in stress with time was recorded. Figure 14 shows the results obtained at a tensile strain of about 0.02. The relaxation behavior at other strain levels has been determined to be essentially the same, which is attributable to the small strain hardening of MERL 76 at this temperature. Two important observations can be made from Figure 14. The first one is that the fracture life of the oil-quenched specimen is very short, less than one hour. In contrast, the air-cooled material has accumulated 23 hours, in several stress relaxations at increasing strains, without failure. The second observation is that the air-cooled material relaxes the stress at a considerably faster rate than the oil-quenched material. This observation can also be illustrated by comparing the stress dependence of the deformation rate during the relaxations which is shown in Figure 15 (note that the deformation rate is proportional to the rate of change in stress). For a given stress, the deformation rate of the oil-quenched material is about one order of magnitude smaller than that of the air-cooled material. However, the stress dependence of the deformation rate in relaxation is about the same for both materials with an exponent of about 16.

The relaxation behavior at lower deformation rates, below about 10^{-3} per hour, could not be obtained from the relaxation experiments because of the rapid fracture and the general experimental difficulties in monitoring the slow relaxation. However, because of the small strain hardening, the stress dependence of the deformation rate in relaxation is expected to be similar to the secondary creep rate. This expectation is verified by results from creep tests either at constant loads or with stresses increased incrementally, which are indicated as datum points and dashed lines, repsectively, in Figure 16. To illustrate the stress dependence of the deformation rate at lower stresses, results from previous creep tests are shown in dotted lines in Figure 16. Note the lower stress dependence of the deformation rate in the case of the oil-quenched material and the smaller difference in creep rates between the air-cooled and the oil-quenched materials at the lower stresses.

Another interesting difference between the air-cooled and the oil-quenched material is in their fracture ductility in creep, stress relaxation and tensile tests. Figure 17 shows the fracture elongations at 704°C. The fracture strain of the oil-quenched material in relaxation is very low, less than 0.004. In contrast, the air-cooled material has accumulated, in several relaxations, a strain of 0.02 without failure. The creep-rupture ductility of the air-cooled material increases slowly with stress and approaches the tensile ductility at high stresses. In comparison, the oil-quenched material has generally lower creep ductility which is relatively insensitive to stress except at low stresses where the creep ductility is low. The divergence of the creep ductility between the oil-quenched and the air-cooled material at high stresses can be correlated with their failure modes; the former fractured transgranularly while the latter intergranularly (see Figure 18).

DISCUSSION

The study of the nature of MERL 76 -325 mesh powder did not reveal any major surprises. Higher interstitial element levels were detected in bulk analyses and by the Auger electron spectrographic analysis of the surface layers of powder. However, these increased concentrations did not influence consolidation characteristics or subsequent mechanical properties. The results for both mesh sizes demonstrated excellent tensile and smooth stress-rupture properties; in general, notch-rupture properties are also good but there was a tendency for mixed results to be found at high stresses. Increasing the grain size of the alloy, not unexpectedly, produces further improvement in rupture properties although occasional examples of lower notch capability were again noted. As the notch-rupture behavior was not explained satisfactorily in the first year of the program, considerable further experimental and analytical work was devoted to this problem in the current second-year effort. The study has concentrated on the MERL 76 conditions used in the first-year study, distinguished on the basis of heat treatment. One condition was air-cooled from 1120°C solution treatment temperature and showed about equivalent smooth and notch properties; the second, oil quenched from the same solution temperature, was extremely 'notch brittle'. The following paragraphs cover the general features of the stress-rupture behavior before considering some of the specific phenomena noted in the Results Section.

Notch Rupture and Stress Relaxation

Under a net-section stress which is smaller than the yield stress, as in the present case, a notched section will deform in a rather complex manner. At a sufficiently high stress, a small volume of material at the notch root deforms plastically, because of the concentrated stress, while the bulk remains elastic. The plastic deformation is accompanied by a stress redistribution by creep processes which reduce the local stresses at the notch root. As the amount of localized plastic deformation increases, the magnitudes of the local stresses decrease toward steady state values determined by the elastic strain in the bulk. Thus, basically, notch rupture is a strain-controlled relaxation phenomenon and a correlation between the notch-rupture behavior and the stress-relaxation properties can therefore be expected. This correlation has indeed been established in the present study. Specifically, the notch-rupture life of MERL 76 has been correlated with the fracture life in stress relaxation of a smooth (Kt=1) specimen. To provide insight into the notch rupture phenomenon, the stress relaxation and creep properties of MERL 76 will be discussed in detail below.

Figure 16 illustrates two significant differences between the air-cool and the oil-quench heat treatments. Firstly, at high stresses, relaxation or creep rates of the oil-quenched material are about one order of magnitude lower than those of the air-cooled material. This difference has two potentially important consequences. The first one is that, as

a result of the higher creep resistance (lower stress relaxation rate), the oil-quenched material will be subject to a high stress for a longer period of time than the air-cooled material. In general, a high tensile stress can contribute to premature fracture by:

(a) rapid nucleation and growth of cavities
(b) grain boundary decohesion
(c) general (grain boundary) damage, reducing stress for overload failure

Factor (a) is inconsistent with the fracture morphology and, therefore, will not be considered further. Fracture by grain boundary decohesion due to the presence of a brittle film, results in very low ductility and occurs at the peak stress with very short rupture life. These characteristics were not observed; although the rupture ductility of the oil-quenched material in stress relaxation is rather low, the fracture did not occur at the highest stress. Grain boundary decohesion in the presence of an aggressive environment will be discussed later. Bulk damage (c) could take the form of (wedge) crack formation at boundaries; a sufficiently large concentration of which would reduce the fracture stress. In the case of a surface nucleated crack, such damage could serve to reduce the critical crack size required for overload failure. Insufficient data has been generated to provide a critical test for this postulate.

The second consequence of the slower stress relaxation rate is related to the accumulation of damage. Since the fracture is intergranular, grain boundary deformation processes are obviously important. The presence of wedge-type cracking suggests that grain boundary sliding is an important damage mechanism, but attempts to find direct evidence of relative grain boundary displacement have not been successful. This may be due to the small grain size (21 μm) and that the critical damage is very small (the <u>total</u> fracture strain of one of the oil-quenched specimens in relaxation is only 0.0025). However, other experimental results, which will be reviewed below, do consistently point to grain boundary sliding as a critical damaging mechanism. These results can be related to current theoretical understanding of the grain boundary sliding mechanism briefly summarized below.

At relatively high temperatures, grain boundaries exhibit many of the characteristics of a viscous fluid and grain boundary motion can be described by Newtonian flow. As a result, the contribution of grain boundary sliding becomes important only at relatively low deformation rates. For grain boundary sliding to occur in a polycrystal, accomodating deformation in the grain matrix is also required. Simultaneous grain boundary sliding and matrix deformation at low stresses result in creep rates faster than those extrapolated from high stresses as indicated in Figure 19. This is a schematic illustration of the relationship between the secondary creep rate and stress derived theoretically by Hart[1] and Crossman and Ashby[2]. At low stresses (region A), grain

boundary sliding is a maximum, independent of stress. The grain boundary sliding contribution decreases as the strain rate (stress) increases through the transition region B to the high stress region C. The transition is characterized by a lower stress dependence of the creep rate and a transition strain rate, $\dot{\gamma}_T$ which is a grain boundary microstructural parameter, given by [2]

$$\dot{\gamma}_T = \frac{1}{A}\left\{\left(\frac{8\delta\omega D_B G}{kTdf_b p^2}\right)^n\right\}^{\frac{1}{(n-1)}} \qquad \ldots\ldots\ldots (1)$$

A is a constant defined in the equation

$$\dot{\gamma}_p = A\left(\frac{\tau}{G}\right)^n \qquad \ldots\ldots\ldots (2)$$

where $\dot{\gamma}_p$ and τ are the shear strain rate and stress; G is the shear modulus; n is the stress exponent; f_b is the area fraction of particles at the grain boundaries; p is the particle diameter; ω is the atomic volume; D_B is the boundary diffusion coefficient; d is the grain diameter and δ is the grain boundary thickness.

For a given material, the transition strain rate can be changed by heat treatments: increasing the grain size, the size and density of particles at the grain boundaries and decreasing the boundary diffusion coefficient, lower the transition strain rate. At the high stress region C where stress relaxation occurs, the grain boundary sliding contribution and hence the propensity for grain boundary damage, depends on the ratio of the deformation rate to the transition strain rate in a manner depicted in Figure 20. The contribution of grain boundary sliding increases rapidly with the decreasing strain ratio and reaches a maximum determined by the stress sensitivity of the strain rate. For materials with a stress exponent of about 16, as in MERL 76, the maximum contribution of grain boundary sliding is about 0.4 [2,3]. Slow deformation rates coupled with a high transition strain rate are conditions favoring grain boundary sliding.

Therefore, the second significant difference between the air-cooled and the oil-quenched materials is an indication of a transition region in the oil-quenched material at lower stresses as illustrated in Figure 16. The transition strain rate is of the order of 10^{-4} per hour. A transition region for the air-cooled material cannot be defined from the existing data but should occur at strain rates lower than those studied. This difference between the two materials can be traced to the grain boundary microstructure. Rapid cooling by oil-quenching produces grain boundaries with lower concentrations of gamma prime and carbide particles compared with those resulting from the slower air-cooling (Figures 9 and 10). Further, the observed transition strain rate can be calculated from equation (1) if the particles which impede the grain boundary motion are assumed to be the gamma prime particles (in addition to carbide particles) and the activation energy for grain boundary diffusion is assumed to be about 52 Kcal/mole. The latter value is slightly below that for the self-diffusion (70 Kcal/mole) and significantly higher than that for grain boundary diffusion 27 Kcal/mole in pure nickel.

These two significant differences between the air-cooled and the oil-quenched materials, shown in Figure 16, can be related to notch-rupture properties if one assumes that the notch fracture is caused by damage due to grain boundary sliding. At high stresses where the relaxation occurs, the strain ratio $\dot{\gamma}_A/\dot{\gamma}_T$ (Figure 20) for the oil-quenched material is more than one order of magnitude larger than that for the air-cooled material. Therefore, for a given amount of strain accumulated during the relaxation, the oil-quenched material sustains a significantly larger amount of grain boundary damage than the air-cooled material (consequently a significantly shorter life). For a given deformation rate the partitioning of strain into grain boundary sliding and intragranular components, according the Crossman-Ashby analysis, is determined by the magnitude of the transition strain rate. Reducing the transition strain rate decreases the accumulation of grain boundary sliding damage (and therefore improving the notch-rupture performance). Equation (1) shows that this can be accomplished by increasing the grain size and/or, more effectively, by decreasing the temperature since D_B varies exponentially with temperature. All these predictions are in general agreement with the test results given in Tables 5 and 7.

Environmental Effects

The environment has been shown to be another critical element of the notch brittleness phenomenon. If the environment is removed, then notch properties are improved by several orders of magnitude and similar increases are found if the first part of a test is performed in a vacuum. This indicates that a damaging environment/grain boundary interaction must occur during the very early stages of stress relaxation. To establish any quantitative model of the stress-rupture process, the specifics of this interaction must be known and integrated with the mechanical parameters. One could speculate that the importance of grain boundary sliding is to expose new surface; the environment could then react, setting up chemical conditions that cause grain boundary decohesion. Such a sequence would account for the importance of strain rate and strain in producing new surface at a critical rate and a high normal stress to cause any boundary separation. If the function of the grain boundary sliding strains is to create damage, this usually occurs at internal locations, such as triple points rather than the surface. Thus, one would have to postulate that the environment diffused along grain boundaries for fracture to occure. Any reader familiar with stress-corrosion phenomena will recognize very similar problems. The basic difficulties in describing the environmental side of the process had led to concentration on defining the mechanical conditions needed to produce fracture. The methodology used is outlined below.

The Definition of Fracture Conditions

The calculation of the local deformation behavior for a curcumferentially notched bar is not a trivial problem. No analytical solution has yet been developed. In the present study, numerical analysis is being used based upon the Neuber's relation for the elastic and the plastic stress-

strain at a notch. Two different results have been obtained depending on the assumptions used. If one assumes that the plastic strain consists of entirely the time-dependent creep, the notch deformation behavior is highly dependent upon the loading rate. High loading rate results in a maximum local stress which is two to three times higher than the nominal (net section) stress and occurs before the maximum nominal stress is reached. High loading rate is also accompanied by high relaxation rates. In contrast, if one assumes that plastic strain also accumulates according to power hardening law, the notch deformation in this case is found to be much less sensitive to the loading rate. These assumptions will be checked by future experiments. When the correct deformation sequence is established, the local stress, strain and strain rates can be calculated for any given time.

If the notch can be demonstrated to fracture after a critical amount of grain boundary sliding at the notch root, the Crossman-Ashby analysis can be used to predict the rupture life, provided the local stress strain behavior can be calculated accurately. The fracture criterion can then be written as:

$$\epsilon^{c}_{GB} = \int_{0}^{t_F} f\left(\frac{\dot{\epsilon}(t)}{\dot{\epsilon}_T}\right) \dot{\epsilon}(t)dt \quad \text{.....(3)}$$

where ϵ^{c}_{GB} is the critical strain to fracture, $\dot{\epsilon}(t)$ is the local deformation rate at the notch and t_F is the rupture time. $f(\dot{\epsilon}/\dot{\epsilon}_T)$ is the strain partition function which has the form shown in Figure 20 and can be approximated by $0.4\,\mathrm{sech}\,(C\dot{\epsilon}/\dot{\epsilon}_T)$ where C is a constant. With the appropriate values of $\dot{\epsilon}(t)$ equation (3) can be integrated numerically to determine ϵ^{c}_{GB} if t_F is known and vice versa.

It is quite possible that the grain boundary sliding strain will prove to be only one criterion that must be satisfied for fracture. As the analysis will also yield information on local stress and strain rate, the criticality of these parameters will be assessed.

The model derived will be tested to explain the stress dependence of the notch-rupture lives of the air-cooled and the oil-quenched materials shown in Figure 13 and the loading rate effect shown in Table 8. An analysis of the effect of loading temperature on notch-rupture life (Table 9) is less tractable since it requires the development of constitutive equations at various temperatures. The beneficial effect of loading at lower temperatures (with the stress maintained during the temperature increase) can be qualitatively understood since the initial relaxation occurs with little or no grain boundary sliding.

Effect of Surface Treatment

It has been observed that shot peening is an effective surface treatment for improving the notch-rupture life of MERL 76 at 704°C. Beneficial effects associated with peening are usually considered to be the compressive residual stresses and the deformation structure. It was thought

that pre-stressing could produce similar effects. However, this assumption was not substantiated (see Table 6). The differences between peening and pre-stressing may be in the magnitude and uniformity of the deformation. Pre-stressing probably results in smaller and less homogeneous deformation than peening.

CONCLUSIONS

The major conclusions that can be drawn from the work performed in the second year of this program are as follows:

1. Characterization of -325 mesh MERL 76 powder revealed several structural features typical of rather rapid cooling. Higher concentrations of interstitial elements were measured for the fine powder compared with the more typically used -80 mesh fraction. These higher levels did not alter the consolidation or grain growth behavior of the material.

2. Mechanical properties determined on HIP consolidated -325 and -80 mesh material revealed no significant differences. HIP above the γ' solvus resulted in a coarser grain size and superior stress rupture capability. In all stress-rupture testing, some scatter in notch properties was found at high stress levels.

3. The notch stress-rupture properties of two conditions of MERL 76 were shown to be a function of microstructure. Quenching from a low solution treatment temperature gave straight grain boundaries, containing a low concentration of precipitates, and resulted in a notch-brittle condition. Air cooling gave more heavily decorated boundaries and a structure that exhibits much less notch sensitivity.

4. A large number of factors were shown to influence rupture behavior in the notch-brittle material. The life could be increased at one test temperature by the following methods:

   - Elimination of the air environment during test. Performing only the first part of a test in a vacuum produced a similar life improvement.
   - Shot peening the notch surface
   - Preloading at lower temperatures before increasing to the test temp.
   - Rapid loading rates

5. Stress relaxation tests on smooth specimens, at initial stresses above the yield, duplicated the notch differences between the two materials. Thus, "notch-brittle" MERL 76 failed after short times with low ductility; the more 'notch-ductile' material did not fail.

6. Creep and relaxation rates for the two materials were also shown to diverge at high stresses. The general shape of the strain rate-stress curves were consistent with theoretical predictions for a material deforming by power law creep and grain boundary sliding.

7. Analytical procedures are outlined that are being applied to give a quantitative description of notch behavior. Finite element methods are used to define local stress, strain and strain rate at notch roots. The achievement of a critical grain boundary strain is the proposed failure criterion which can be calculated using the appropriate strain partition function.

ACKNOWLEDGEMENTS

The authors would like to thank A. E. Gemma, J. T. Hill, and R. N. Weber for their assistance in the numerical calculation of the stress and strain in a notch and F. T. Nardozzi for experimental assistance.

In addition, several most helpful discussions held with Professor R. Raj are acknowledged.

REFERENCES

1. E.W. Hart: Acta Met., 1967, Vol. 15, p. 1545.

2. F.W. Crossman and M.F. Ashby: Acta Met., 1975, Vol. 23, p. 425.

3. M.V. Speight: Acta Met., 1976, Vol. 24, pp. 725 - 729.

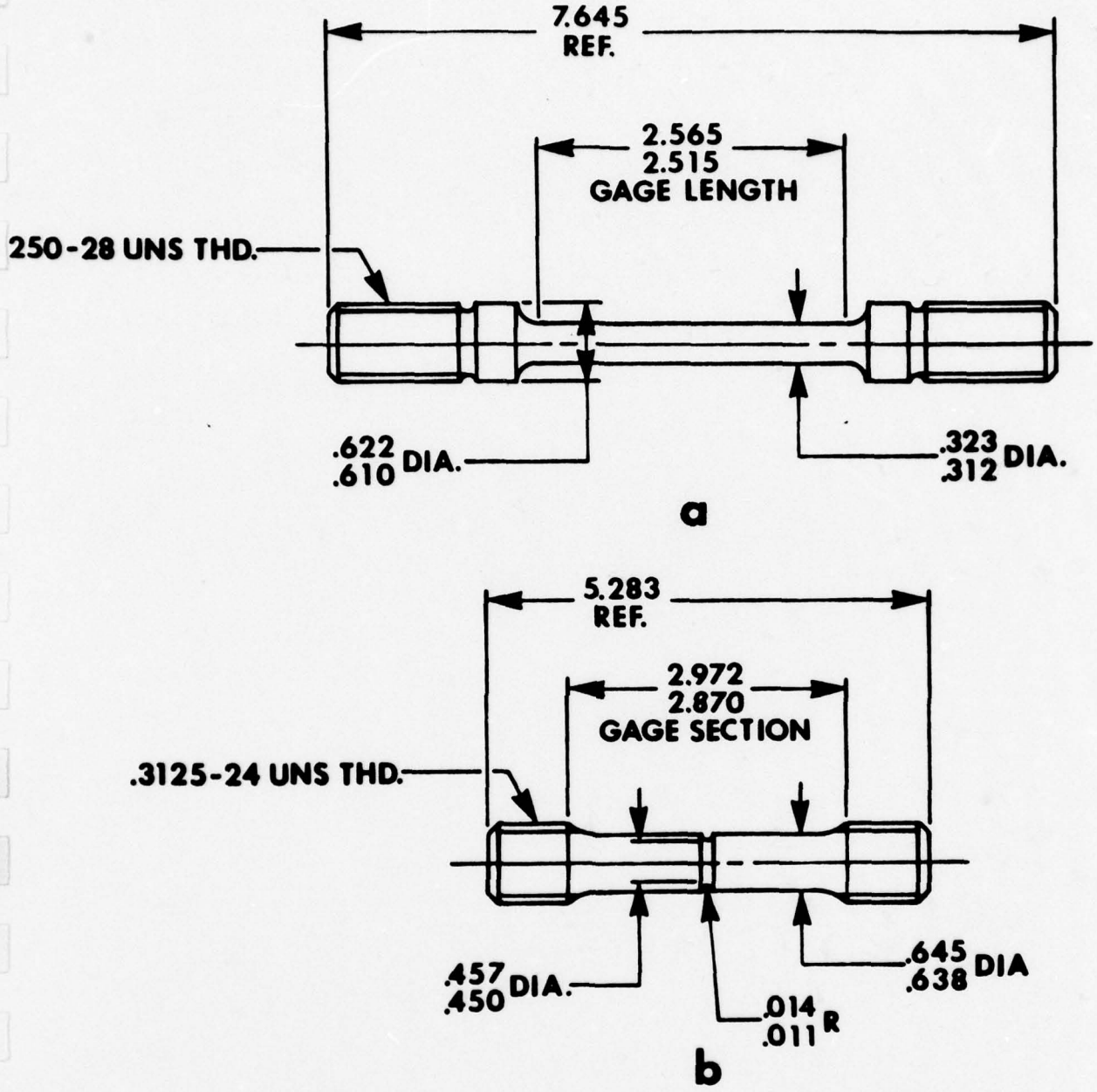

Figure 1. Dimensions of (a) creep-rupture specimen (b) notch-rupture specimen, in cm.

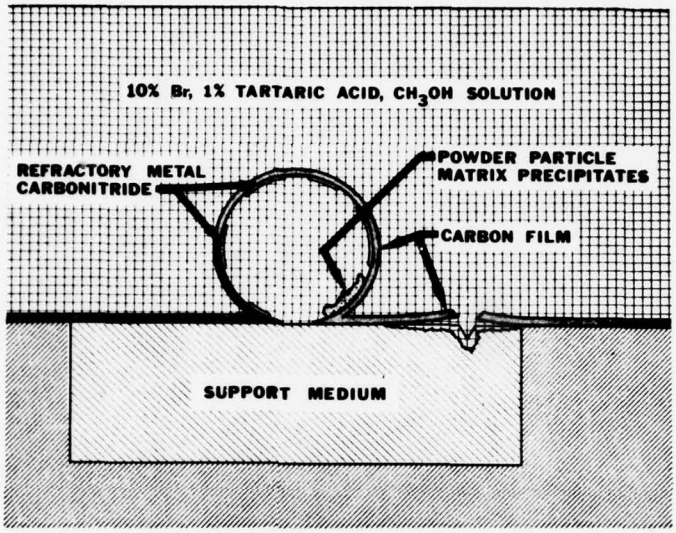

Figure 2. Schematic illustration of a powder particle extraction replica technique (courtesy of P. Genereux).

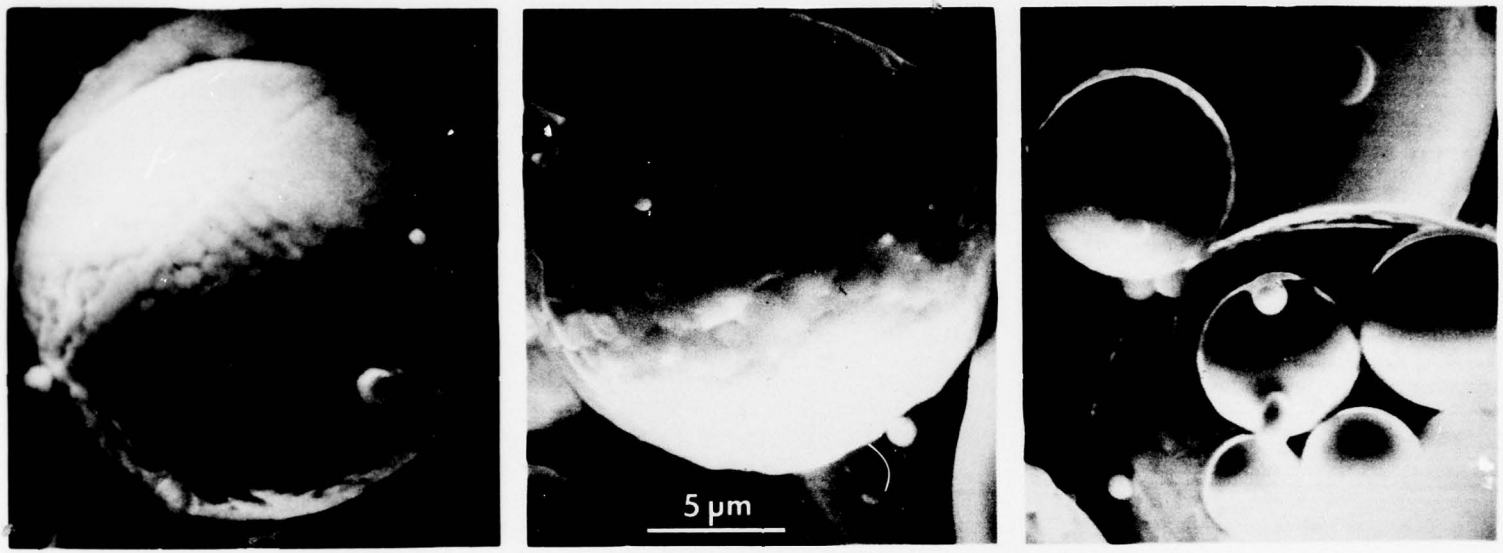

Figure 3. Surface morphologies of the -325 mesh MERL 76 powder particles (a) dendritic (b) granular (c) featureless.

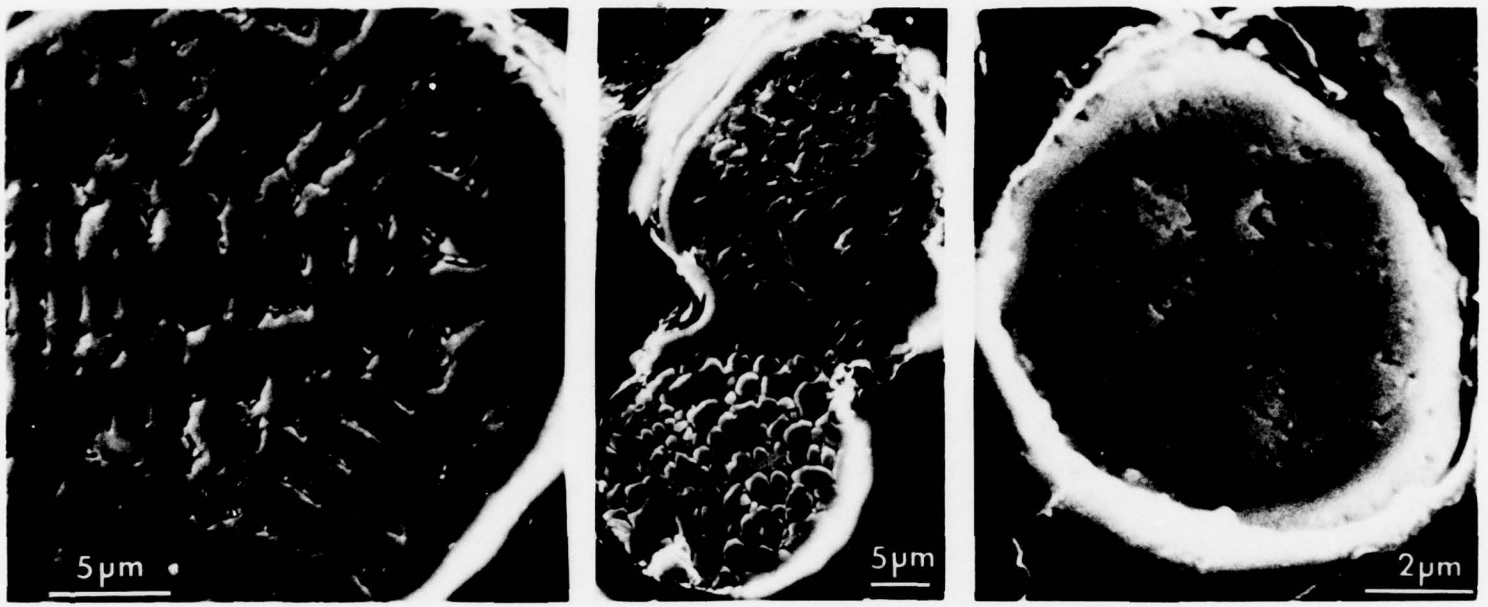

Figure 4. Microstructures of the -325 mesh MERL 76 powder particles (a) dendritic (b) bottom particle - granular, top particle - a mixed granular and dendritic (c) a mixed granular and dendritic core surrounded by a segregation-free surface layer.

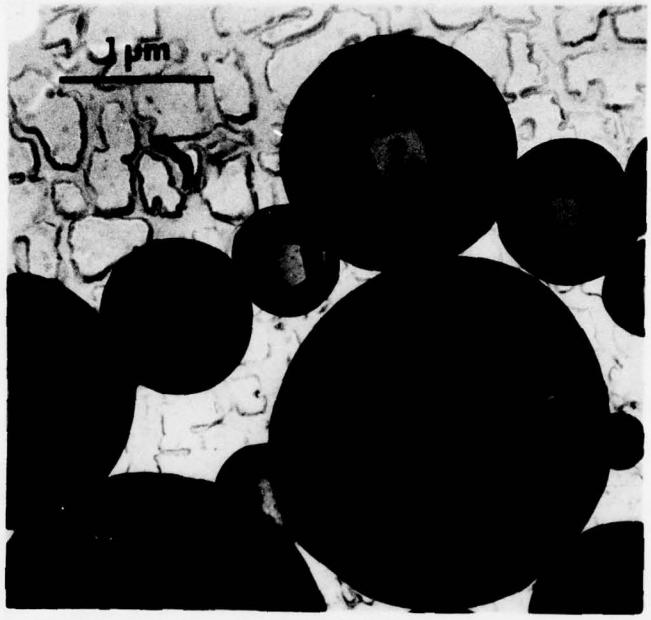

Figure 5. Extraction replica from the -325 mesh MERL 76 powder particles showing a small number of equiaxed particles extracted from the surfaces of the powder particles. The light regions within the spheres are areas where the replica are in contact with the substrate.

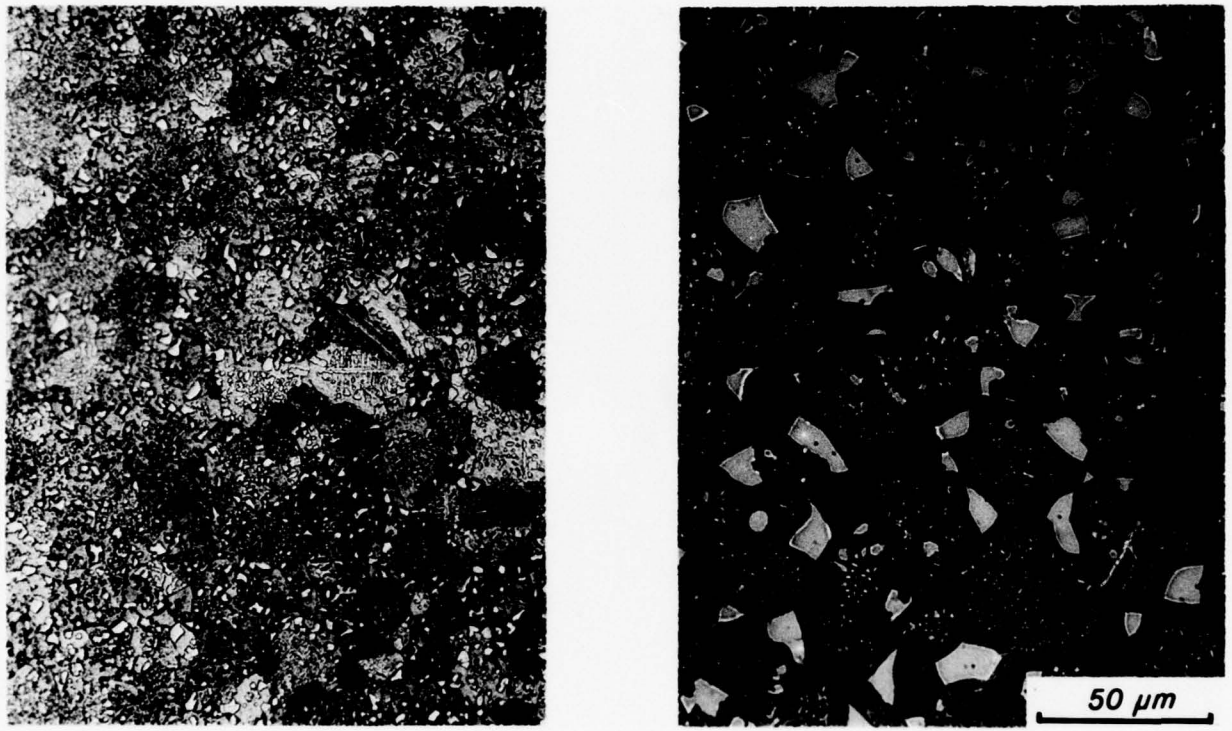

Figure 6. Microstructures of MERL 76 consolidated from (a) -325 mesh powder (b) -80 mesh powder.

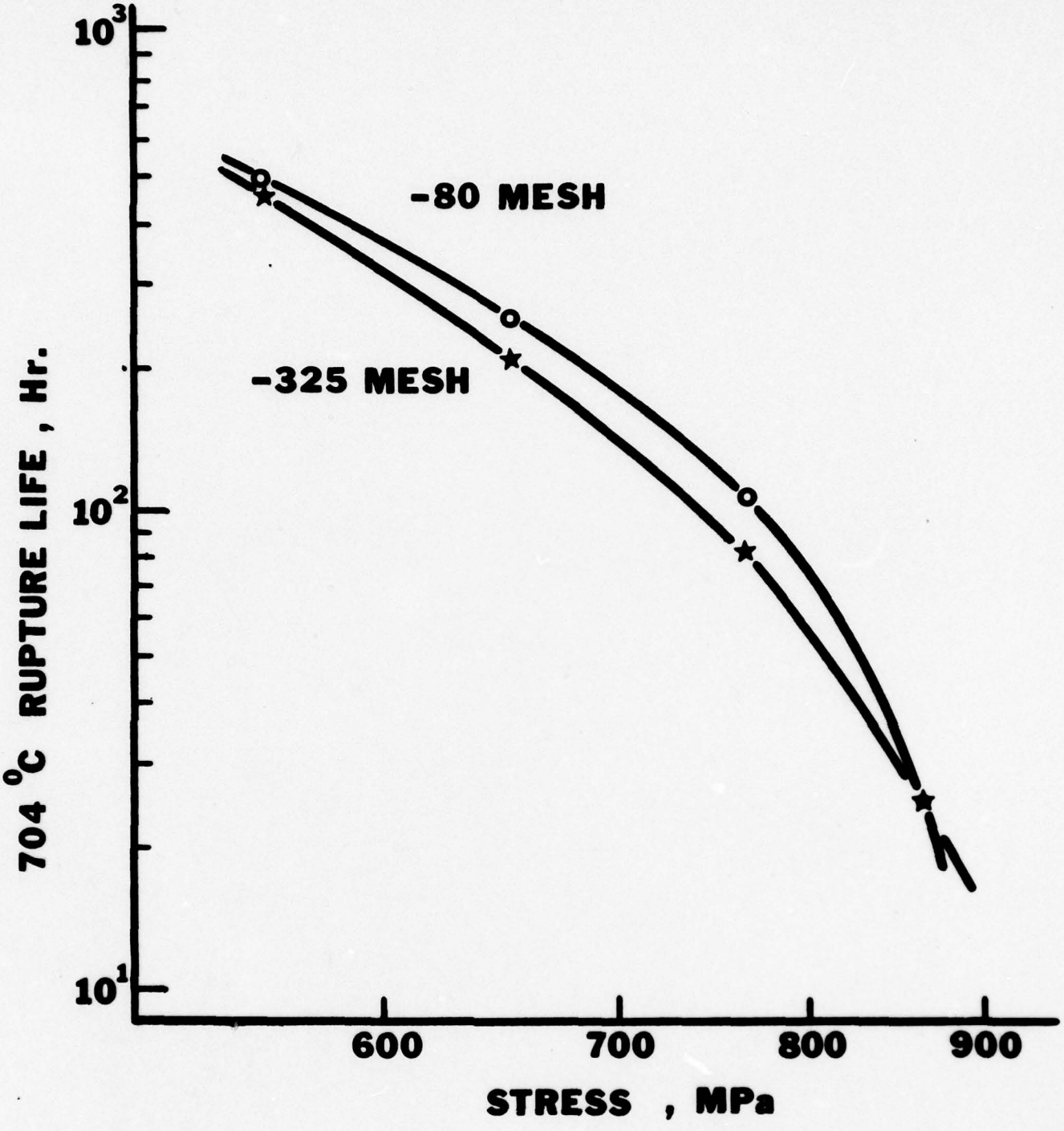

Figure 7. Stress-rupture lives of smooth (K_t=1) MERL 76 specimens at 704°C. The materials were HIP-consolidated from -80 mesh and -325 mesh powders at 1177°C. Heat treatment: 1120°C/2 Hr./AC + 760°C/8 Hr./AC.

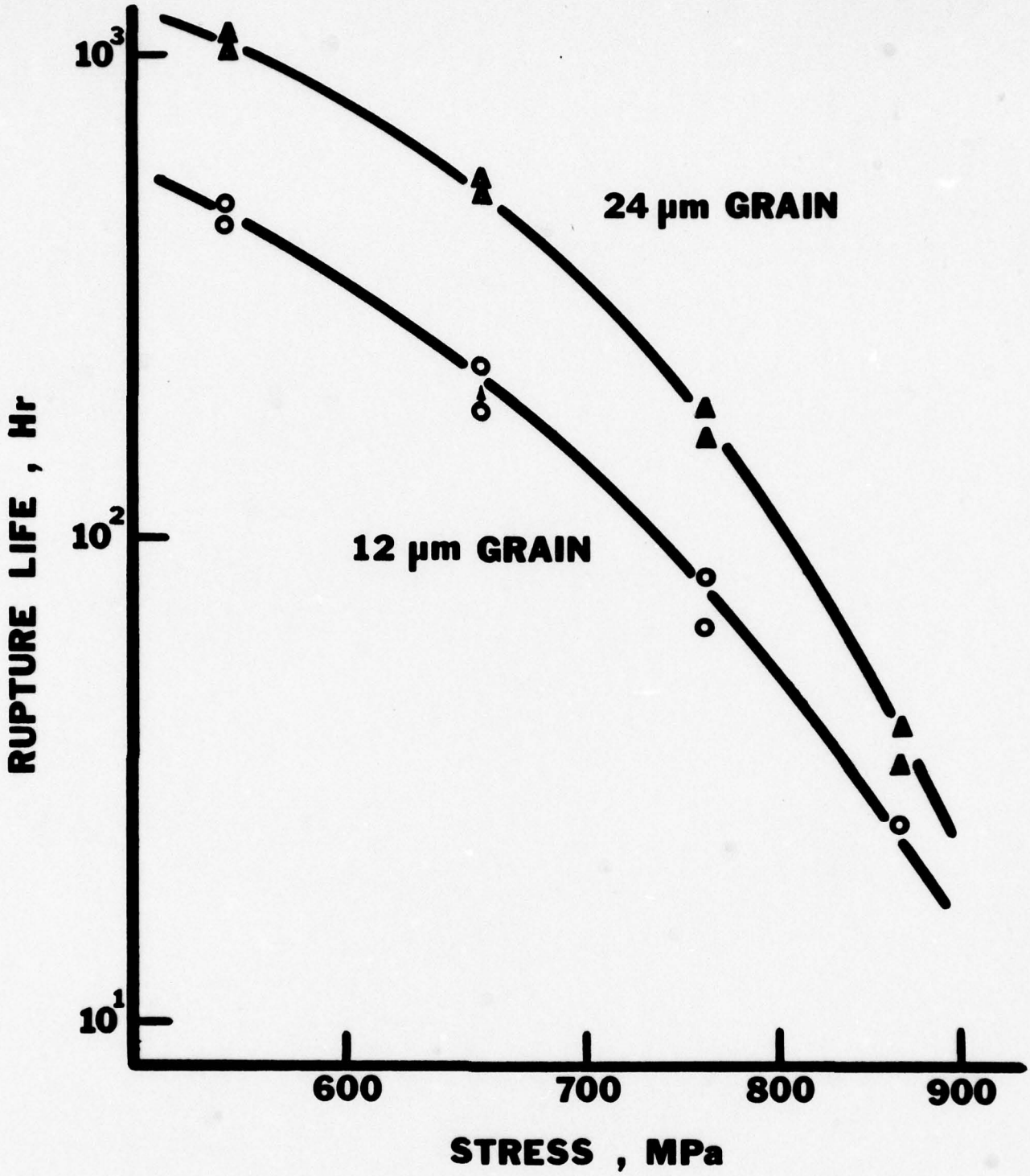

Figure 8. Stress-rupture lives of smooth (K_t=1) MERL 76 specimens at 704°C. The materials were HIP-consolidated from -325 mesh powder at 1177°C and at 1195°C which resulted in grain sizes of 12 µm and 24 µm, respectively. Heat treatment: 1163°C/2 Hr./Furnace Cooled to 1130°C/OQ + 870°C/40 min./AC + 980°C/45 min./AC + 650°C/24 Hr./AC + 760°C/8 Hr./AC.

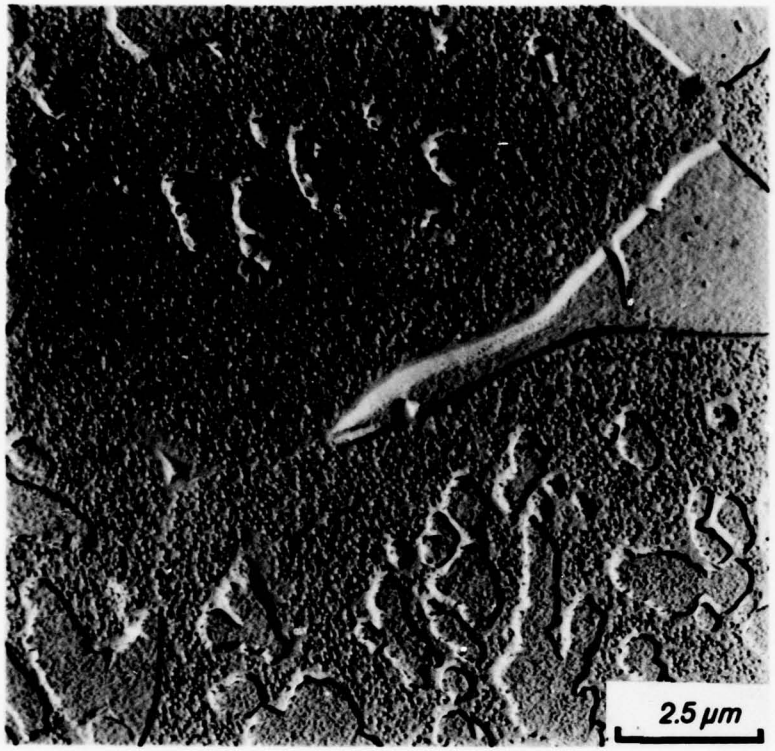

a

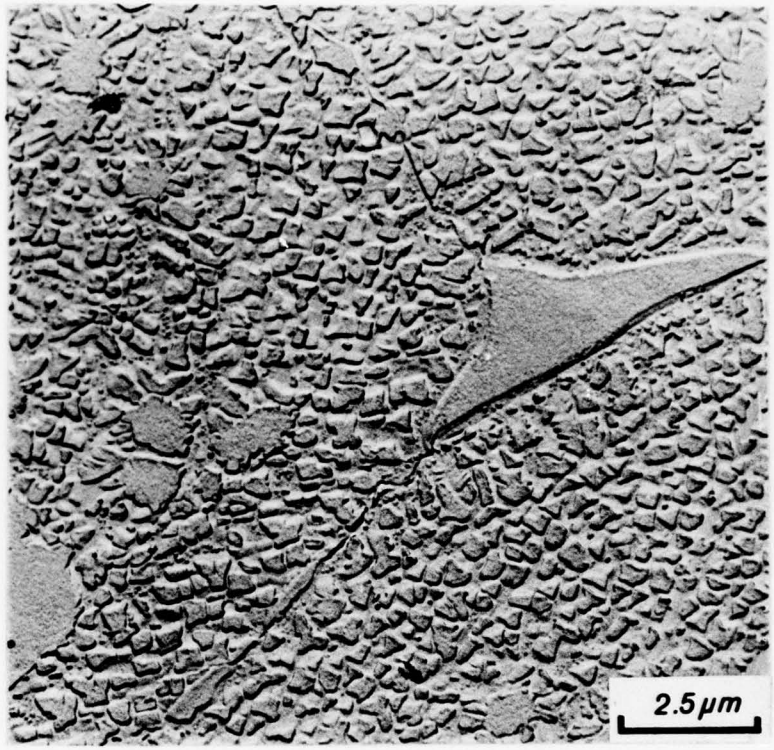

b

Figure 9. Microstructures of MERL 76 after two different heat treatments (a) 1120°C/2 Hr./OQ + 760°C/8 Hr./AC, (b) 1120°C/2 Hr./AC + 760°C/8 Hr./AC.

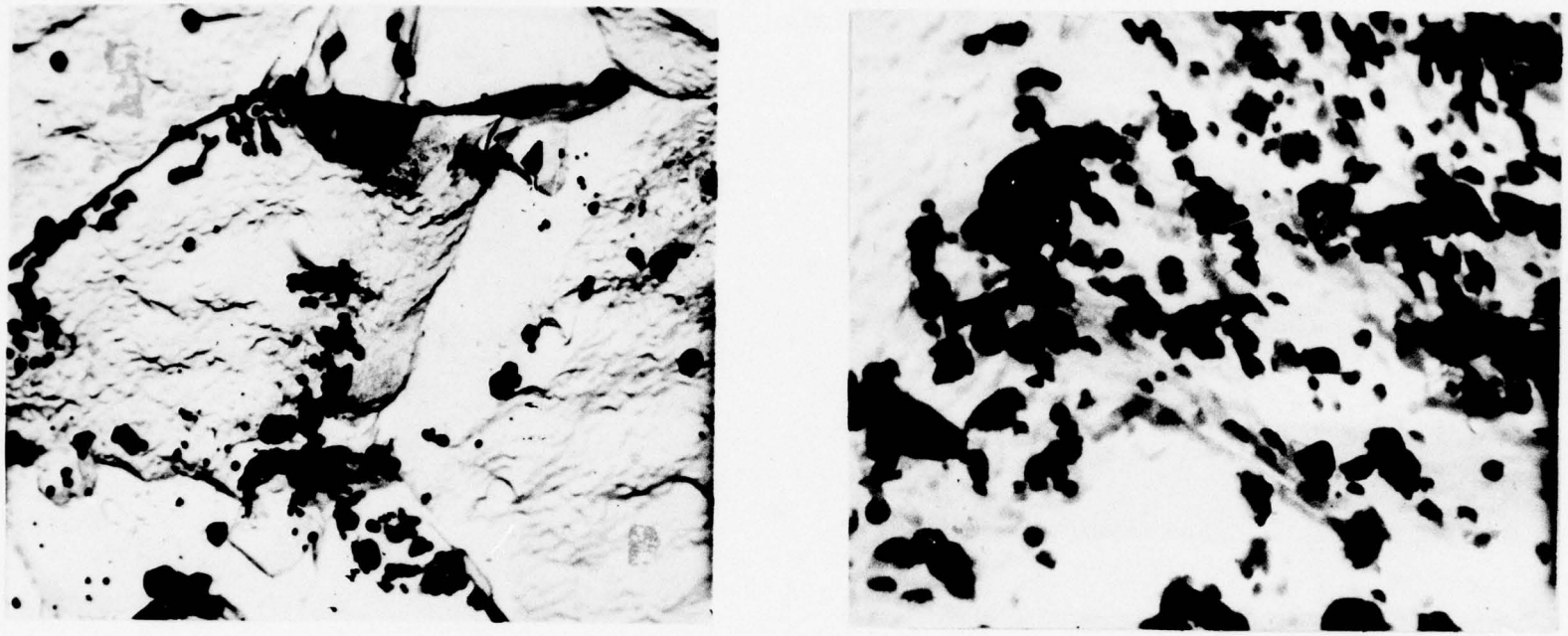

a

b

Figure 10. Particles extracted from MERL 76 (a) 1120°C/2 Hr./OQ + 760°C/8 Hr./AC (b) 1120°C/2 Hr./AC + 760°C/8 Hr./AC.

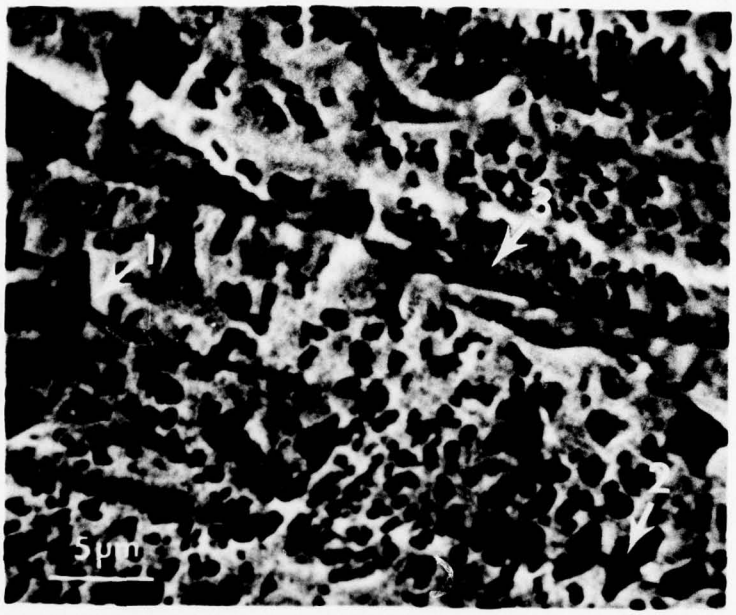

Figure 11. Scanning electron micrograph of the gage area of a MERL 76 notched specimen (K_t = 3.8) illustrating three different crack nucleation sites: 1. primary gamma prime/matrix interface 2. primary gamma prime particle 3. machining mark (normal to stress axis). Specimen was tested at 704°C/690 MPa for 111 hours in a vacuum. Heat treatment: 1120°C/2 Hr./AC + 760°C/8 Hr/AC.

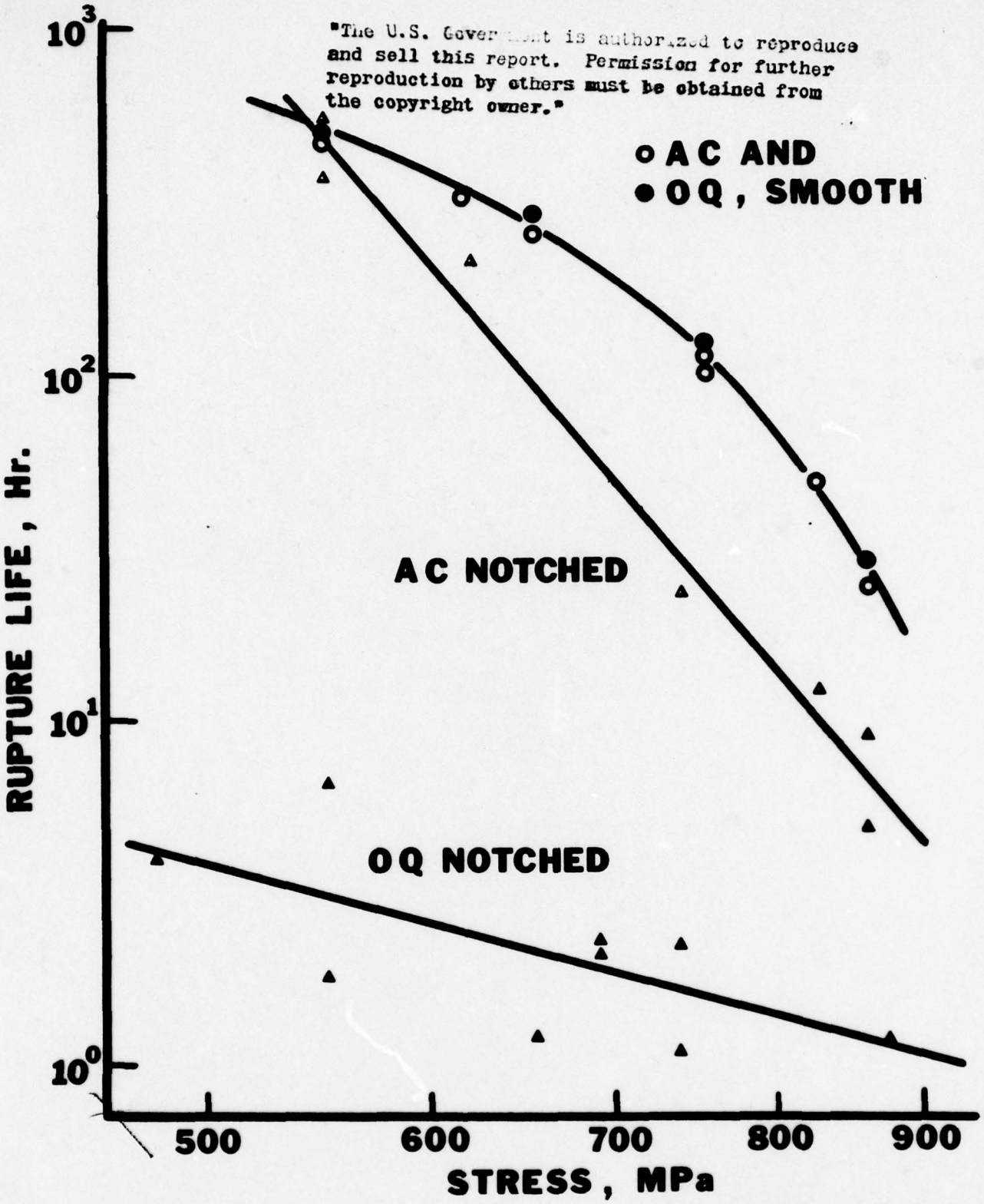

Figure 13. Stress-rupture lives of smooth (K_t=1) and circumferentially notched (K_t=3.8) MERL 76 specimens at 704°C. Heat treatment: (AC) 1120°C/2 Hr./AC + 760°C/8 Hr./AC,(OQ) 1120°C/2 Hr./OQ + 760°C/8 Hr./AC.

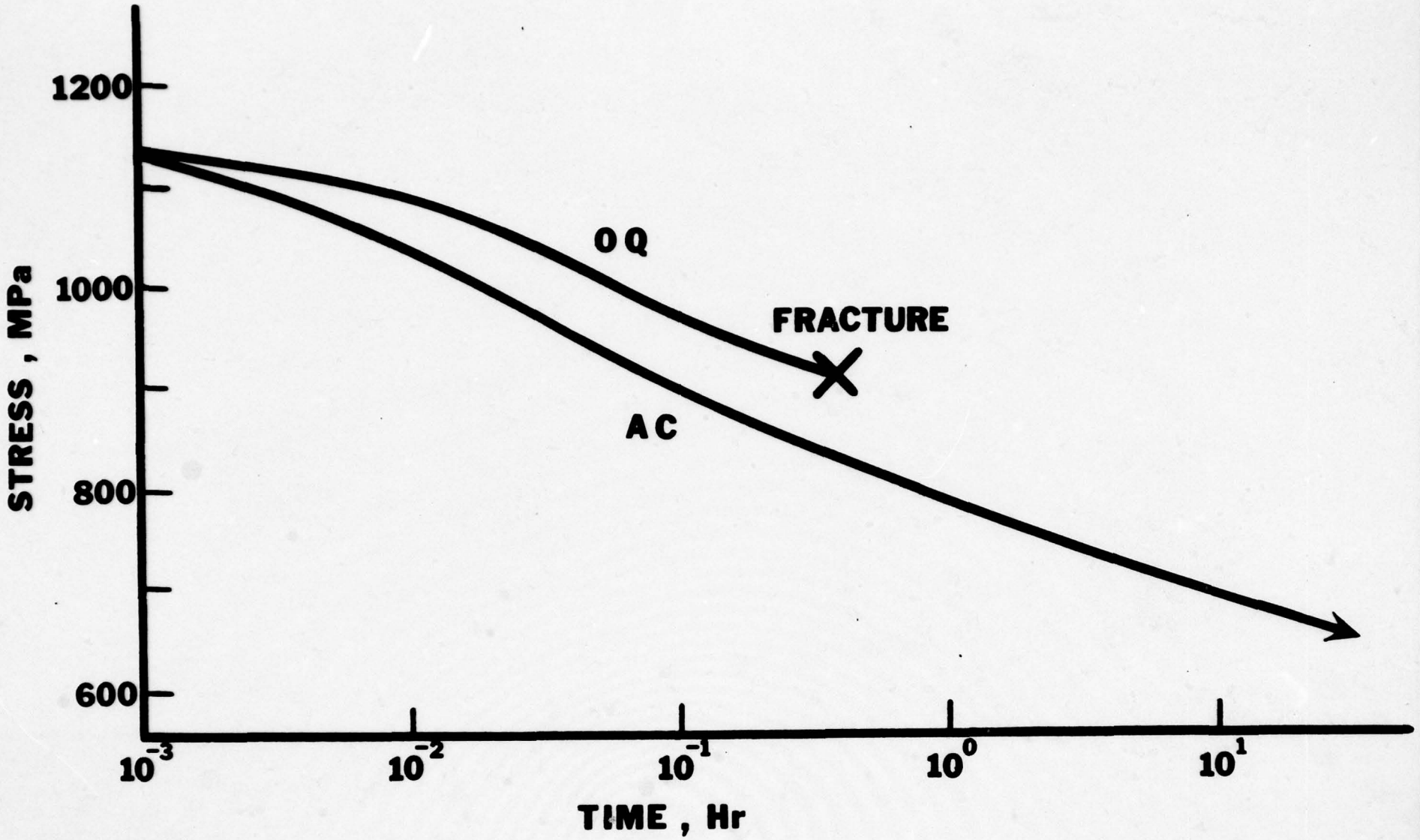

Figure 14. Stress relaxation behavior of MERL 76 at 704°C. Heat treatment: (AC) 1120°C/2 Hr./AC + 760°C/8 Hr./AC,(OQ) 1120°C/2 Hr./OQ + 760°C/8 Hr./AC.

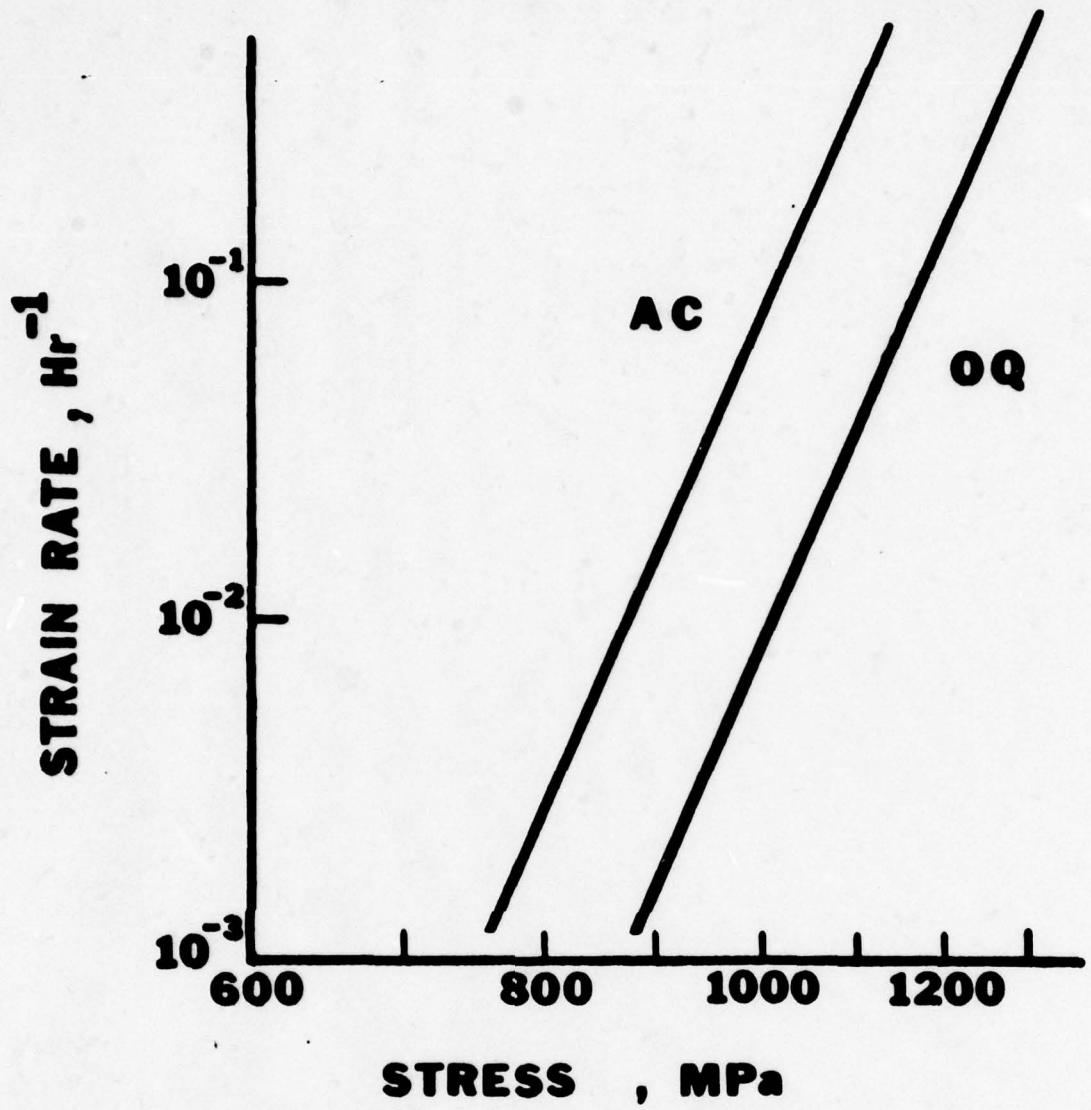

Figure 15. Relaxation strain rate versus stress for MERL 76 at 704°C. Heat treatment: (AC) 1120°C/2 Hr./AC + 760°C/8 Hr./AC, (OQ) 1120°C/2 Hr./OQ + 760°C/8 Hr./AC.

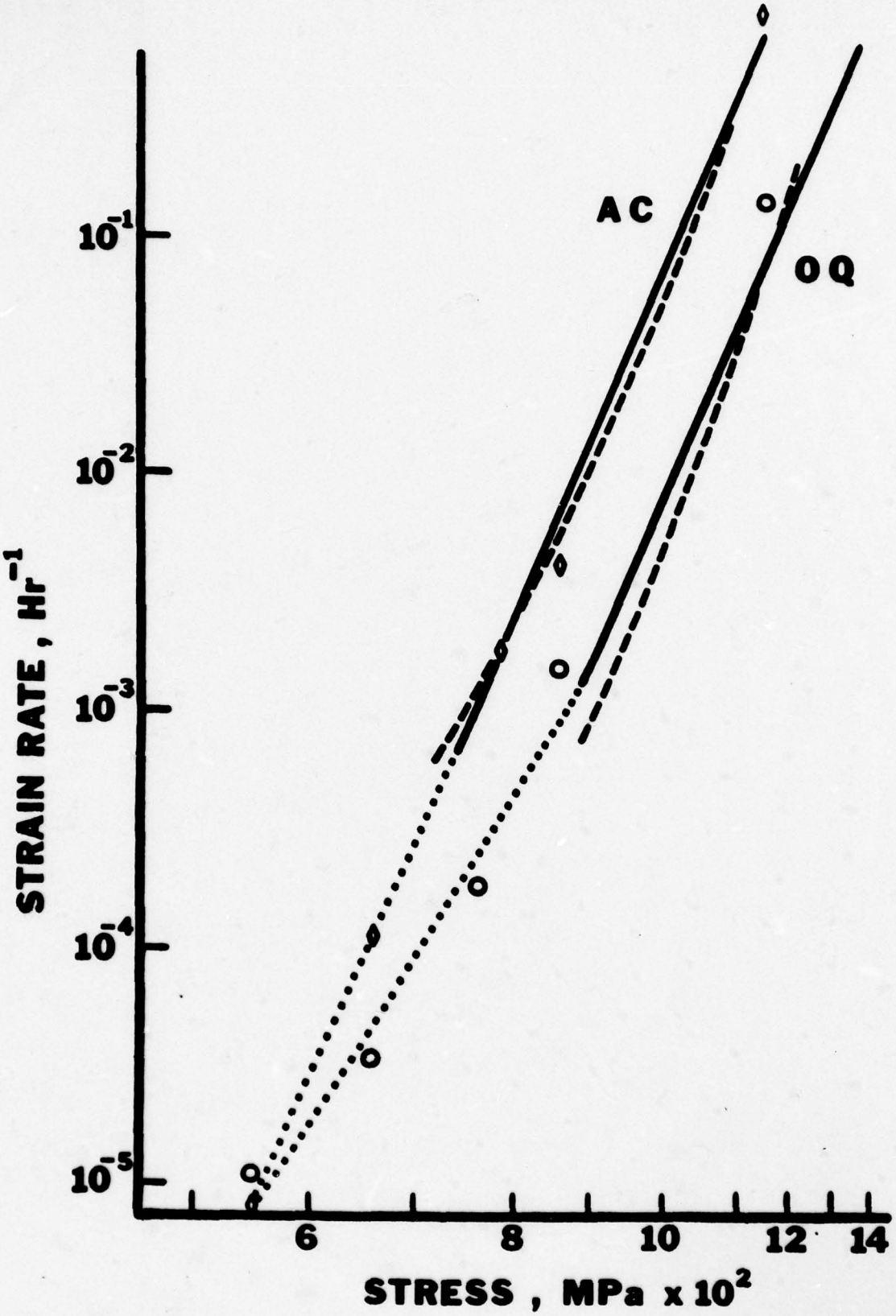

Figure 16. Strain rate versus stress for MERL 76 at 704°C. The solid lines represents the stress relaxation data. The dashed lines represent data from creep tests in which the stresses were incrementally increased. The datum points and the dotted lines represent data from constant load creep tests. Heat treatment: (AC) 1120°C/2 Hr./AC + 760°C/8 Hr./AC, (OQ) 1120°C/2 Hr./OQ + 760°C/8 Hr./AC.

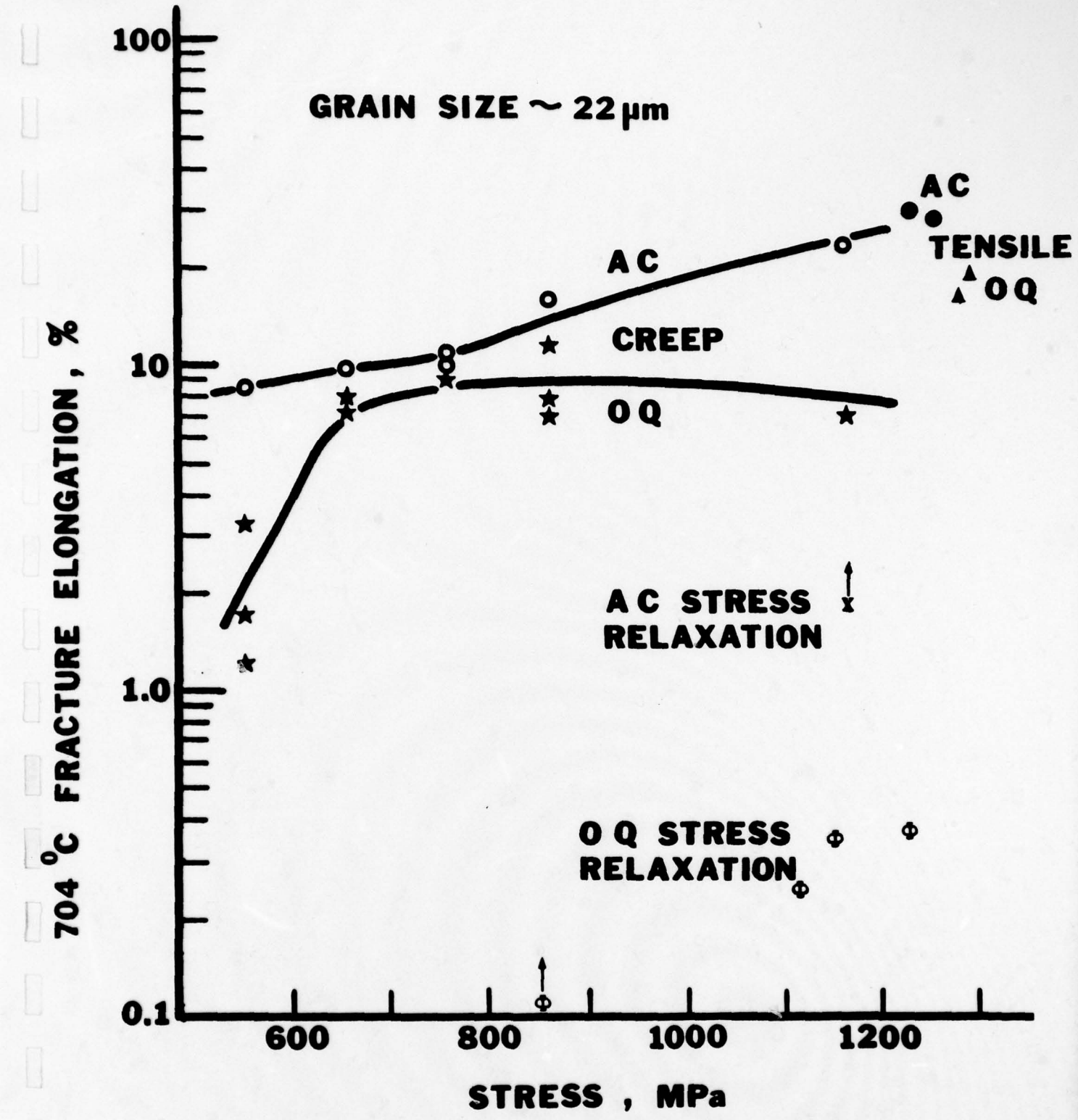

Figure 17. Fracture elongation of MERL 76 in creep, stress relaxation and tensile tests at 704°C. Heat treatment: (AC) 1120°C/2 Hr./AC + 760°C/8 Hr./AC, (OQ) 1120°C/2 Hr./OQ + 760°C/8 Hr./AC.

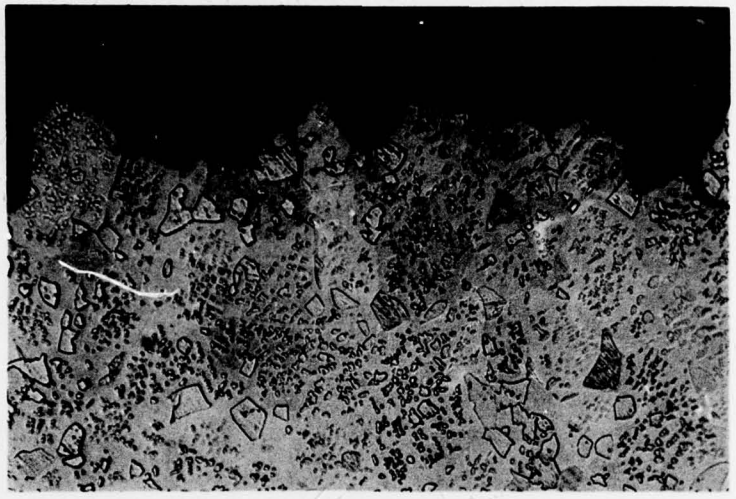

a

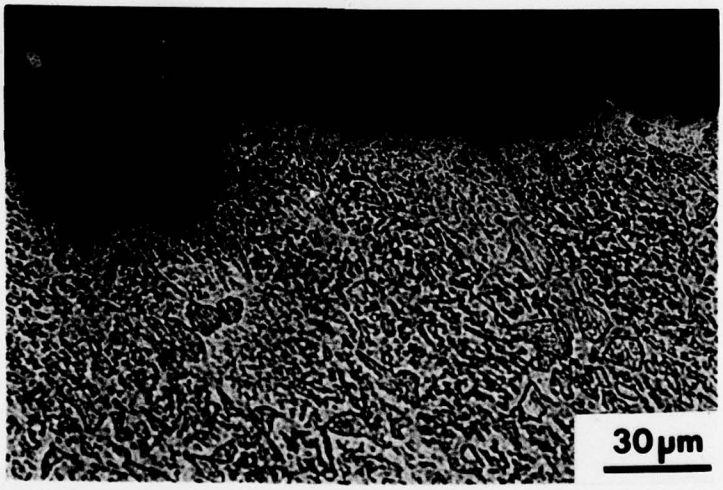

b

Figure 18. Appearance of the creep rupture in MERL 76 at 704°C/ 1165 MPa (a) 1120°C/2 Hr./OQ + 760°C/8 Hr./AC (b) 1120°C/2 Hr./ AC + 760°C/8 Hr./AC

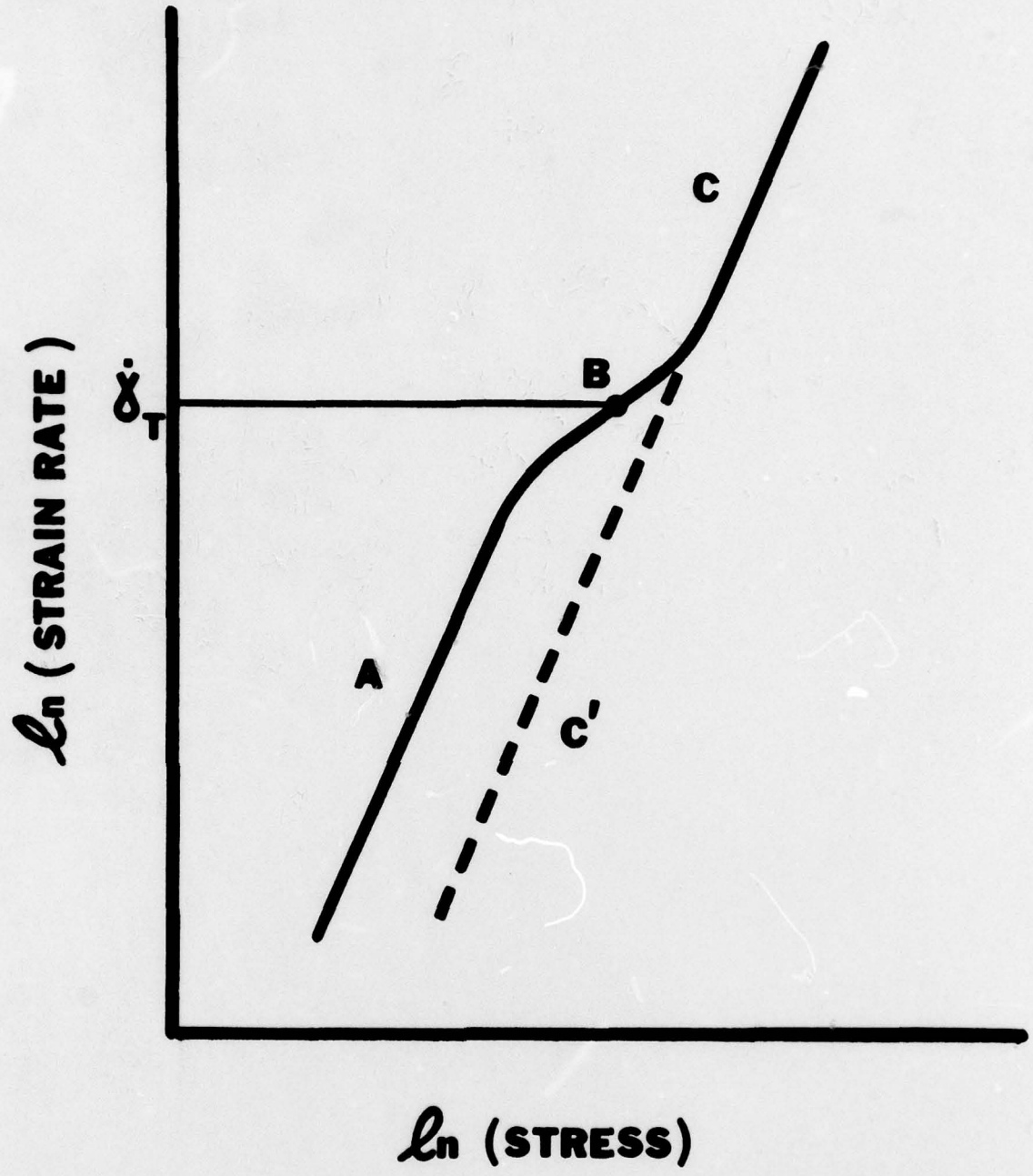

Figure 19. Schematic representation of the secondary creep rate versus stress. In the low stress region A, the grain boundary sliding contribution reaches a maximum, independent of stress. The simultaneous deformation by grain boundary sliding and intragranular mechanism results in creep rates faster than those extrapolated from the high stress region, C'. Grain boundary sliding contribution decreases rapidly in the high stress region C. Region B is the transition region which can be characterized by a transition strain rate $\dot{\gamma}_T$ (2).

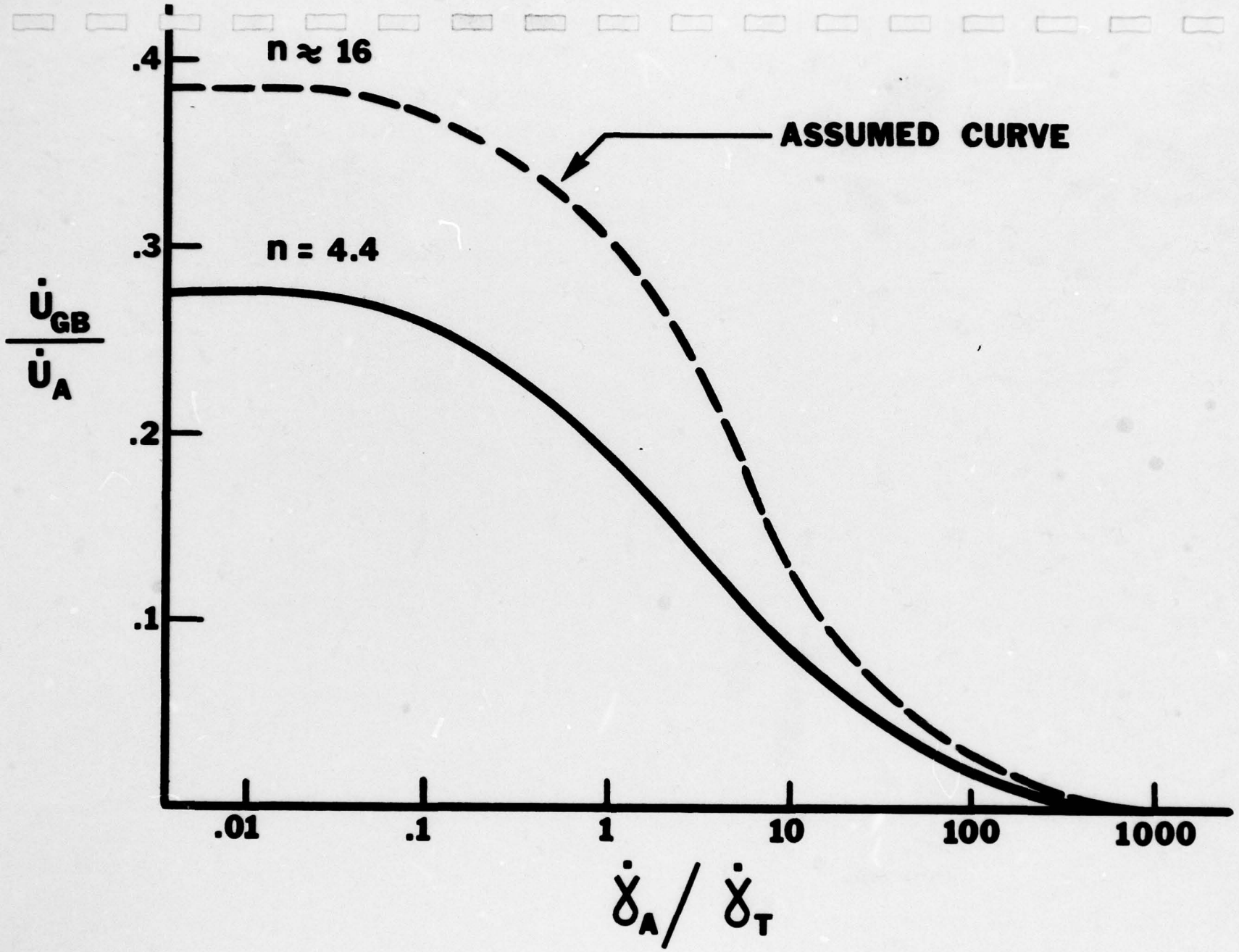

Figure 20. The contribution of grain boundary sliding as a function of deformation strain rate, $\dot{\gamma}_A$ and the transition strain rate, $\dot{\gamma}_T$, Ref. 2. The assumed behavior for MERL 76 which has a stress exponent of about 16 is illustrated by the dashed line.

TABLE 1

OXYGEN AND NITROGEN CONTENTS
(ppm) IN -80 MESH AND -325 MESH
MERL 76

Material	-80 Mesh		-325 Mesh	
	O	N	O	N
Loose Powder	123	*	175	13
Consolidation	99	13	151	21

* No Data

TABLE 2

COMPOSITIONS OF MERL 76
(WEIGHT %)

	-80 Mesh	-325 Mesh
Ni	Bal.	Bal.
Cr	12.3	12.1
Co	17.9	18.1
Mo	3.3	3.2
Al	5.0	5.1
Ti	4.3	4.3
Nb	1.7	1.6
Hf	0.74	0.58
B	0.018	0.020
Zr	0.06	0.07
C	0.025	0.026
O	94 ppm	151 ppm
N	30 ppm	21 ppm

TABLE 3

704°C TENSILE PROPERTIES OF
-80 MESH AND -325 MESH MERL 76*

Mesh	0.2%YS MPa	UTS MPA	El %	RA %
-80	983.2	1247.1	29.3	40.1
-325	1033.5	1227.1	19.0	22.1

* 1120°C/2 Hr./AC + 760°C/8 Hr./AC.

TABLE 4

704°C STRESS-RUPTURE PROPERTIES OF
-80 MESH AND -325 MESH MERL 76*

Stress MPa	-80 Mesh				-325 Mesh			
	Life Hr.	El %	RA %	Notch Life Hr.	Life Hr.	El %	RA %	Notch Life Hr.
550	488.7	13.0	14.1	375.0	390.6	4.1	5.8	175.3
					523.8	4.1	5.6	198.3
655	253.3	9.7	12.3	120.0	208.2	2.9	5.0	110.0
					206.9	4.6	6.1	129.3
758	115.0	11.0	15.8	23.5	86.7	7.2	10.3	4.9
	100.9	10.2	12.0		82.7	6.7	11.6	73.5
860	24.8	16.1	20.9	4.9	25.1	8.7	13.9	50.5
				9.0	24.3	7.6	13.0	22.7

* HT: 1120°C/2 Hr./AC + 760°C/8 Hr./AC

TABLE 5

EFFECT OF GRAIN SIZE ON 704°C
STRESS-RUPTURE PROPERTIES
OF -325 MESH MERL 76

	Grain Size 12μm				Grain Size 24μm			
Stress MPa	Life Hr.	El %	RA %	Notch Life Hr.	Life Hr.	El %	RA %	Notch Life Hr.
550	450.6 498.4	3.9 4.7	5.2 7.0	213.9 192.3	1030.0 1130.6	1.7 1.2	1.9 -	842.4 1000.5 +
655	184.9 + 229.3	* 8.7	* 9.4	120.0 110.0	547.9 537.6	7.3 7.6	10.8 12.4	598.6 518.0
758	64.8 83.8	4.7 8.7	6.2 9.9	69.5 6.3	161.5 198.7	8.9 9.1	17.0 10.6	345.2 6.2
860	26.0	9.0	13.5	0.3 4.2	33.9 41.2	11.5 7.8	14.7 11.7	3.1 152.1

HT: 1163°C/2 Hr./Furnace Cool To 1130°C/OQ
+ 870°C/0.7 Hr./AC + 980°C/0.8 Hr./AC
+ 650°C/24 Hr./AC + 760°C/8 Hr./AC

+ Test terminated with no failure

* Thread failure

TABLE 6

EFFECT OF SURFACE TREATMENT
ON NOTCH-RUPTURE LIFE OF
MERL 76* AT 704°C/690 MPa

Surface Treatment	Life, Hr.
As-Machined	2.3
As-Machined	2.1
Electropolished	0.5
As-Machined + Prestrained**	
827 MPa at 20°C	0.5
690 MPa at 370°C	1.7
As-Machined + Peened (11.5N)	95.0 +
As-Machined + Peened (6.5N)	113.0 +

* HT: 1120°C/2 Hr./OQ + 760°C/8 Hr./AC

** The stress was released during the subsequent temperature increase to 704°C.

\+ Test terminated with no failure.

TABLE 7

EFFECT OF TEMPERATURE ON NOTCH-RUPTURE LIFE (HR.) OF MERL 76 AT 690 MPa

Temperature (°C)	Heat Treatment* OQ	AC
538	808.9 + 860.7 +	1000 +
650	860.8 + 10.9	1000 +
704	2.1 2.3	72
788	0.1 0.7	2.2 3.4

* HT: 1120°C/2 Hr./AC + 760°C/8 Hr./AC
1120°C/2 Hr./OQ + 760°C/8 Hr./AC

+ Test terminated with no failure

TABLE 8

EFFECT OF LOADING STRESS RATE
ON NOTCH-RUPTURE LIFE OF MERL 76*
AT 704°C

Stress Rate MPa/Min.	Max. Stress MPa	Life Hr.
825	550	1.8
825	550	6.6
4135	550	255.0
33070	550	91.0 +
2.4	690	1.3
920	690	2.3
920	690	2.1
8,270	690	0.6
41,340	690	0.8
413,400	690	1.7

* HT: 1120°C/2 Hr./OQ + 760°C/8 Hr./AC

+ Test terminated with no failure

TABLE 9

EFFECT OF LOADING TEMPERATURE ON
NOTCH-RUPTURE LIFE OF MERL 76* AT
704°C/690 MPa

Loading Temp.** °C	Life at 704°C Hr.
20	115 +
370	94 +
482	92 +
538	5.0
704	2.3
704	2.1

* HT: 1120°C/2 Hr./OQ + 760°C/8 Hr./AC

** Specimens were held at 690 Mpa for 0.5 hours at the loading temperatures. The stress was maintained during the subsequent temperature increase to 704°C.

\+ Test terminated with no failure.

TABLE 10

EFFECT OF TEST ENVIRONMENT ON
NOTCH-RUPTURE LIFE OF MERL 76* AT
704°C/690 MPa

Environment	Life, Hr.
Air	2.3
Air	2.1
Vacuum, 10^{-5} Torr	178.5 +
Vacuum, 10^{-5} Torr	559.0 +
Tested 6 Hr. in vacuum followed by air test	104.5 +

* HT: 1120°C/2 Hr./OQ + 760°C/8 Hr./AC

+ Test terminated with no failure